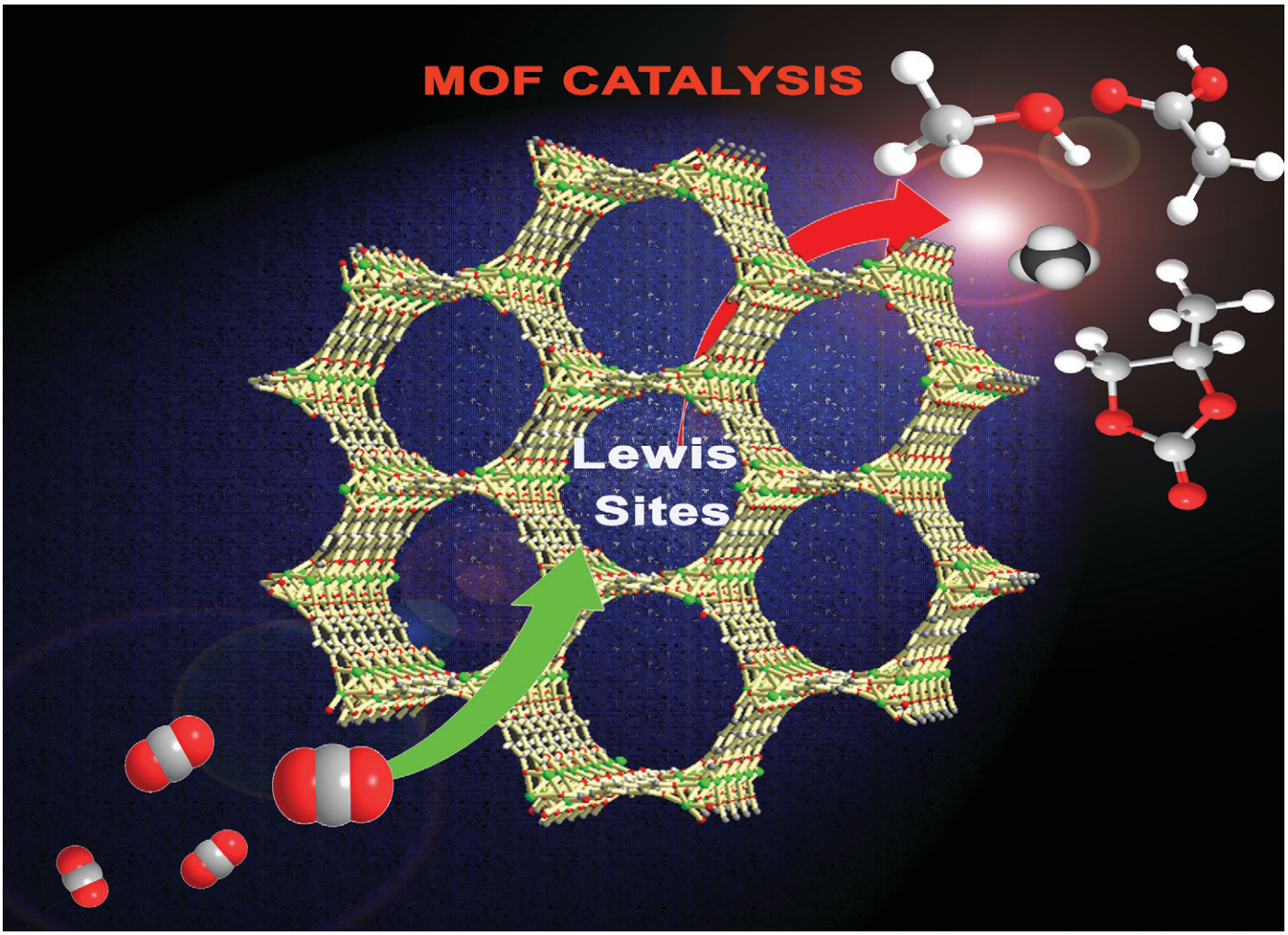


**Showcasing a highlight by Zhigang Hu and Dan Zhao* from Zhao's Group (http://cheed.nus.edu.sg/stf/chezhao/home.html) at National University of Singapore (Republic of Singapore).**

Metal–organic frameworks with Lewis acidity: synthesis, characterization, and catalytic applications

Marked by high porosity, tunable internal surface functionality and concentrated metal sites, metal–organic frameworks (MOFs) are believed to act as the next generation catalytic materials. In this highlight, we review the recent development in the design and synthesis of MOFs with Lewis acidity, and their applications in heterogeneous catalysis.

## As featured in:


See Zhigang Hu and Dan Zhao, *CrystEngComm*, 2017, **19**, 4066.

ROYAL SOCIETY OF CHEMISTRY

rsc.li/crystengcomm

Registered charity number: 207890

CrystEngComm

HIGHLIGHT

View Article Online
View Journal | View Issue



Cite this: *CrystEngComm*, 2017, **19**, 4066

# Metal–organic frameworks with Lewis acidity: synthesis, characterization, and catalytic applications

Zhigang Hu and Dan Zhao*

Received 30th December 2016,
Accepted 7th February 2017

DOI: 10.1039/c6ce02660e

rsc.li/crystengcomm

Metal–organic frameworks (MOFs) are exquisitely architected through the pervasive coordination bonds between inorganic metal nodes and organic ligands. Marked by high porosity, tunable internal surface functionality, and concentrated metal sites, they are believed to act as the next generation adsorbent and catalytic materials. In particular, the presence of unsaturated metal centers and electron-deficient groups, capable of acting as Lewis acid sites, has made MOFs highly promising in heterogeneous catalysis applications. In this Highlight, we review the recent development in the design and synthesis of MOFs with Lewis acidity, the characterization techniques of Lewis acid sites, and their applications in heterogeneous catalysis.



## 1. Introduction

Metal–organic frameworks (MOFs), also known as porous coordination polymers (PCPs) or porous coordination networks (PCNs), are exquisitely architected through the pervasive coordination bonds between inorganic metal nodes and organic ligands.[1] Marked by high porosity, tunable internal surface functionality, and concentrated metal sites, MOFs are believed to act as the next generation adsorbent[2,3] and catalytic materials.[4] Due to the presence of large amounts of unsaturated metal centers (UMCs), MOFs can inherently act as Lewis acid catalysts.[5] The first example using a MOF as a Lewis acid catalyst was reported by Fujita and co-workers in 1994.[6] They synthesized a Cd–bipyridine MOF and studied its clathration ability with *o*-dibromobenzene and the cyanosilylation reaction of benzaldehyde with cyanotrimethylsilane. Afterward, MOFs have been widely attempted for various reactions, such as cyanosilylation,[7–10] ring opening reaction,[11] Mukaiyama-aldol reaction,[8] Knoevenagel condensation,[12,13] redox reaction,[14–17] $CO_2$ fixation,[18] *etc.* Besides Lewis acidity, the presence of Brønsted acidity in some MOFs greatly expands their catalytic applications.[19–21] Nevertheless, some other issues need to be resolved for their practical applications in catalysis, such as their weak framework stability, diffusion limits, *etc.*[22,23]

*Department of Chemical and Biomolecular Engineering, National University of Singapore, 4 Engineering Drive 4, 117585, Singapore. E-mail: chezhao@nus.edu.sg*

**Zhigang Hu**

*Zhigang Hu obtained his PhD degree in Chemical Engineering from the National University of Singapore in 2016 under the supervision of Dr Dan Zhao. He is now a postdoctoral fellow of Dr Dan Zhao's group, focusing on the synthesis of functional metal–organic framework composites and the establishment of instrumental set-up for MOF-based applications in gas separation, heterogeneous catalysis, and membrane technologies.*

**Dan Zhao**

*Dan Zhao received his PhD degree from Texas A&M University in 2010 under the guidance of Professor Hong-Cai Zhou. After completion of a two-year postdoctoral work at Argonne National Laboratory, he joined the National University of Singapore in 2012 as an Assistant Professor. His research interests include advanced porous materials and their applications in storage, separation, sensing, catalysis, and membrane technologies.*

So far, many excellent reviews regarding MOFs as heterogeneous catalysts have been presented.[24–27] This Highlight will mainly focus on presenting the recent development in the synthetic strategies, characterization techniques, and typical catalytic reactions of MOFs with Lewis acidity whereas not all the synthetic strategies and reaction types can be covered herein. In the first part, we describe the common strategies to construct MOFs with Lewis acid sites, such as defect creation, incorporation of external Lewis acids, post-synthetic methods, *etc.* In the second part, we summarize the characterization techniques currently applied to characterize the Lewis acidity in MOFs, including temperature-programmed gas desorption, infrared spectroscopy, gas adsorption, and theoretical calculation. Thirdly, we briefly review the major reactions catalysed by MOFs with Lewis acidity, such as addition, reduction, oxidation, cyclization, substitution, hydrogenation, host–guest interaction, *etc.* Lastly, we will present the conclusions and outlooks for MOFs as Lewis acid catalysts.

## 2. Synthetic strategies

Unsaturated metal centers (UMCs), which originate from the removal of terminally coordinated solvent molecules on the metal sites or coordinative defects because of missing linkers or clusters, are the major active sites in MOFs for Lewis acid based catalytic reactions.[28] Besides, post-synthetic methods by incorporating or attaching moieties with Lewis acidity also help introduce Lewis acid sites into MOFs.[29]

### 2.1 MOFs with UMCs

The inherent Lewis acidity contributed by UMCs in MOFs can be exemplified by HKUST-1 (HKUST = Hong Kong University of Science and Technology) and MOF-74.[30] These MOFs exhibit strong interactions with polar gas molecules due to the presence of UMCs, as evidenced by their high isosteric heats of adsorption.[31] Another example is $Mn_3[(Mn_4Cl)_3(BTT)_8(CH_3OH)_{10}]_2$ ($H_3BTT$ = 1,3,5-benzenetristetrazol-5-yl), wherein $Mn^{2+}$ is exposed after solvent removal, serving as the Lewis acid sites for size-selective catalysis of cyanosilylation of aromatic aldehydes and Mukaiyama-aldol reactions (Fig. 1).[8] Besides Mg, Cu, and Mn, other metals in MOFs can also generate UMCs, such as Ni, Co, Zr, Fe, Zn, *etc.*[32–34] In this strategy, the formation of UMCs depends on the nature of metal clusters and coordination topology with multidentate ligands.

### 2.2 Incorporation of external moieties with Lewis acidity

Besides the *in situ* synthesis of MOFs with UMCs, externally incorporating functional moieties with Lewis acidity can be another effective way to prepare MOFs for heterogeneous catalysis.[35] For example, Feng and co-workers presented a one-pot strategy to integrate metal-tetrakis(4-carboxyphenyl)-porphyrin (M-TCPP) ligands into UiO-66(Zr) (UiO = University of Oslo).[36] The resultant composite materials maintained the parent crystal structure, morphology, and stability. The one

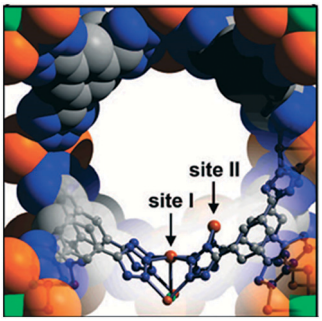


Fig. 1 Schematic illustration of the crystal structure of $Mn_3[(Mn_4Cl)_3(BTT)_8(CH_3OH)_{10}]_2$ showing two types of open $Mn^{2+}$ sites exposed to porous channels.[8] Reprinted with permission from the American Chemical Society, copyright 2008.

incorporated with FeCl-TCPP demonstrated efficient catalytic oxidation of 2,2′-azino-bis(3-ethylbenzothiazoline-6-sulfonic acid) in the presence of $H_2O_2$. However, the control of loading amount and distribution of active moieties remain challenging due to the constraints pressed by pore size, geometry, and compatibility (Fig. 2).

### 2.3 Defect engineering

Defect engineering is an effective way to create Lewis acid sites inside MOFs, wherein the defect concentrations and compensating groups can be systematically tuned.[37] UiO-66 has attracted great attention in tuning its defect concentration[38,39] or even eliminating defected sites.[40] However, most of the reported studies are supported only by a powder X-ray diffraction (PXRD) technique, which is not straightforward in elucidating the crystal structures. Using a single-crystal X-ray diffraction (SXRD) technique, Trickett and co-workers proved that the missing linker defects in UiO-66(Zr) were a result of water molecules binding directly to the zirconium centers.[41] Cliffe and co-workers systematically manipulated the defect distribution and correlated the nanoscale disorder in UiO-66(Hf) (Fig. 3).[42] In our previous work, we developed a modulated hydrothermal (MHT) synthetic approach, which was capable of synthesizing new Zr- and Hf-MOFs with structural defects.[43–45] A good control of ordered defects can be seen in MHT-synthesized NUS-6 (NUS = National University of Singapore),[21,46] whose formation is a result of both missing linkers and clusters in the parental UiO-66-type frameworks.

### 2.4 Post-synthetic metal exchange

The metal nodes of MOFs can be substituted by other metal cations in order to tune their Lewis acidity.[47] Post-synthetic metal exchange is one such approach that can be used to synthesize new MOFs, which cannot be directly synthesized conventionally. For example, Brozek *et al.* demonstrated that the $MZn_3O(O_2C^-)_6$ clusters in $Zn_4O$(1,4-benzenedicarboxylate)$_3$ (MOF-5) could serve as hosts for $V^{2+}$ and $Ti^{3+}$ (Fig. 4).[48] Other MOF-5 analogues featuring $Cr^{2+}$, $Cr^{3+}$, $Mn^{2+}$, and $Fe^{2+}$ sites substituted at the $Zn^{2+}$ nodes were also prepared. They found

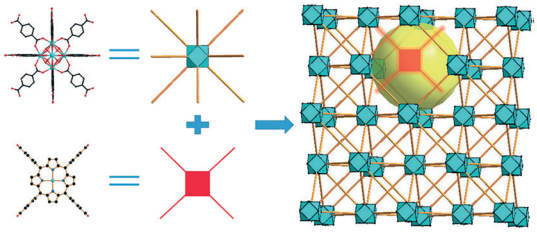

Fig. 2 Schematic illustration of UiO-66 incorporating external Zr-TCPP Lewis acid sites.[36] Reprinted with permission from Wiley, copyright 2016.

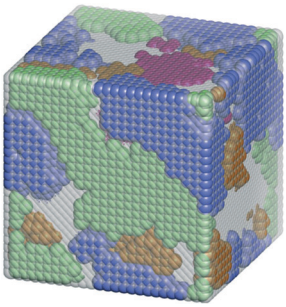

Fig. 3 Atomistic presentation of defect nanoregions in UiO-66(Hf).[42] Reprinted with permission from Macmillan Publishers, copyright 2014.

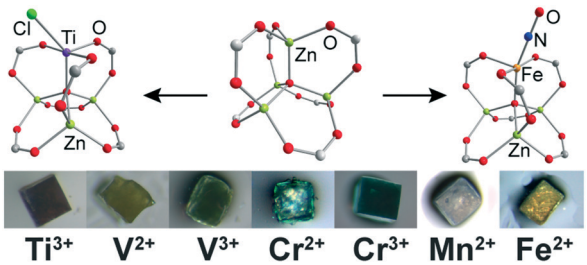


Fig. 4 Illustration of the metal nodes ($Zn^{2+}$) in MOF-5 that can be substituted by $Cr^{2+}$, $Cr^{3+}$, $Mn^{2+}$, and $Fe^{2+}$.[48] Reprinted with permission from the American Chemical Society, copyright 2013.

that the exchanged metal cations were coordinated under an all-oxygen trigonal ligand field and could be reached by both inner- and outer-sphere oxidants. $Cr^{2+}$-MOF-5 was converted into $Cr^{3+}$-substituted MOF-5, while $Fe^{2+}$-MOF-5 activated NO to produce an unusual Fe-nitrosyl complex. Lau *et al.* reported the $Ti^{4+}$ substituted UiO-66 for enhanced $CO_2$ uptake because of the increased Lewis acidity of $Ti^{4+}$ compared to $Zr^{4+}$.[49]

### 2.5 Post-synthetic exchange and metalation

Metalation can be an effective way to endow MOFs with extra metal sites and also Lewis acidity if the building ligands have functional groups, such as hydroxyl and thiol groups.[29] Cohen and co-workers have presented several studies on post-synthetic exchange and metalation (PSEM) in MOFs.[50–52] For example, two steps are involved in one recent study: (1) post-synthetic exchange of 2,3-dithiol functionalized BDC ligands into UiO-66 to produce UiO-66-(2,3) $(SH)_2$; (2) using palladium precursors to complete metalation (Fig. 5). Such metalation with palladium afforded unprecedented Pd-mono(thiocatecholato) moieties within the resultant MOF, which was used as a catalyst for regioselective functionalization of the $sp^2$ C–H bond.

### 2.6 Ligand truncation

Tuning the symmetry of ligands may also generate vacant metal sites.[53] For example, Liu *et al.* used $C_2$-symmetric ligands to replace $C_3$ symmetric ligands and successfully obtained a series of PCN-305-type MOFs (Fig. 6).[54] In our previous study, we synthesized HKUST-1 using mixed isophthalic acid and benzene-tricarboxylic acid (BTC) ligands and obtained a hierarchical porous MOF, HP-CuBTC-0.25, with a mesopore size of around 3.9 nm.[10] Because of the enlarged pore size and increased Lewis acidity caused by defects, HP-CuBTC-0.25 demonstrated a better catalytic performance than pristine HKUST-1 in catalysing the ring-opening reaction of styrene oxide to 2-methoxy-2-phenylethanol and the cyanosilylation reaction of benzaldehyde to cyanohydrins.

### 2.7 MOFs with electron deficient ligands

Besides MOFs with UMCs exhibiting Lewis acidity, many MOFs with electron-deficient moiety-based ligands, such as 7,7,8,8-tetracyano-*p*-quinodimethane (TCNQ),[55] anhydride,[56] and triazine,[57] can also be tailored for potential catalytic applications. For example, Shimomura and his coworkers prepared a MOF with TCNQ-based ligands and it exhibited a H–π-type interaction with benzene, which led to the selective separation of benzene from cyclohexane (Fig. 7).[55] Ghosh and his coworkers prepared two MOFs based on electron-deficient anhydride and triazine ligands for benzene/cyclohexane separation.[56,57] MOFs with this kind of Lewis site remain to be further probed for Lewis acid catalytic applications in the future.

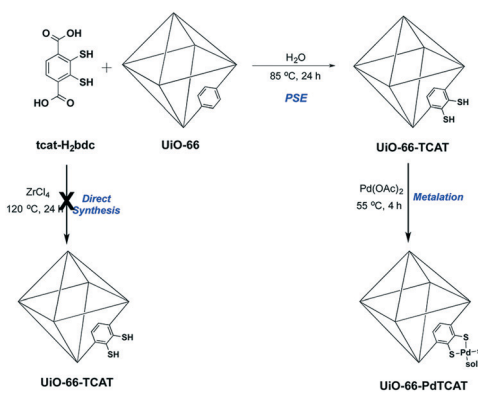


Fig. 5 Schematic illustration of the synthesis of UiO-66-TCAT and UiO-66-PdTCAT *via* the PSEM process.[50] Reprinted with permission from the American Chemical Society, copyright 2015.

 

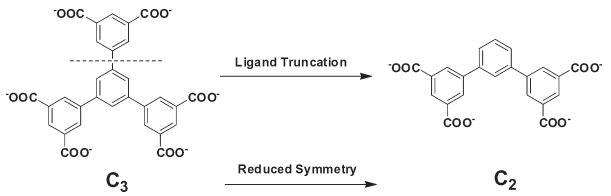


Fig. 6 Schematic illustration of the reduced symmetry ligand derived from a "ligand truncation" strategy for isostructural MOF synthesis.[54] Reprinted with permission from Wiley-VCH, copyright 2013.

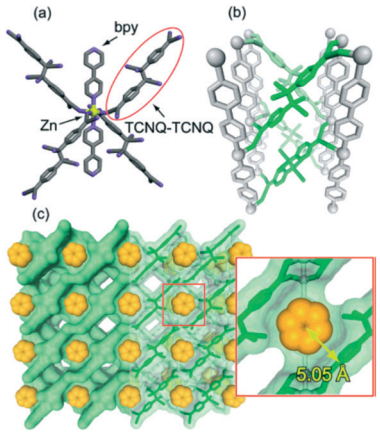


Fig. 7 Scheme of Lewis acidity in MOFs originating from an electron-deficient TCNQ ligand.[55] (a) Coordination environment of Zn(II) ion of **Zn(μ4-TCNQ-TCNQ)bpy**_benzene. (b) TCNQ dimer (green) connected to four 1D chains of Zn and bpy (gray). (c) Benzene arranged in the cage of the undulating channel of **Zn(μ4-TCNQ-TCNQ)bpy**_benzene. Reprinted with permission from the American Chemical Society, copyright 2007.

# 3. Characterization techniques

## 3.1 Temperature-programmed desorption

Temperature-programmed desorption (TPD) is currently one of the most widely adopted techniques to identify the type and density of acid sites in solid catalytic materials such as alumina, amorphous silica–alumina, and zeolites.[58] This technique involves the adsorption of a chosen molecular probe (gas molecule) at a low temperature $T_0$ (excluding physical adsorption) and measuring the rate of its desorption as the temperature increases.[59]

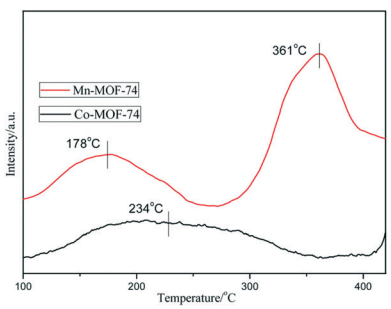


Fig. 8 $NH_3$-TPD spectra of Mn-MOF-74 and Co-MOF-74.[60] Reprinted with permission from the American Chemical Society, copyright 2016.

Currently, $NH_3$-TPD is the most widely used one due to its simplicity and capability of titrating weak acid sites.[61] Jiang *et al.* probed the acid site distributions of Mn-MOF-74 and Co-MOF-74 using this method (Fig. 8).[60] In principle, the higher the desorption temperature, the stronger the acidity. The spectra in the above example indicated two different sorption sites in Mn-MOF-74: a strong site (361 °C) and a weak site (178 °C), while Co-MOF-74 had only one moderate acid site (234 °C). It is notable that TPD using $NH_3$ as the probe often overestimates the quantity of acid sites because of the small molecular size of $NH_3$ (2.9 Å) allowing it to penetrate in almost all the accessible pores of the porous solids and possible additional $NH_3$ adsorption due to $NH_3$–$NH_3$ interactions.[62]

## 3.2 Infrared spectroscopy

Besides $NH_3$, large non-reactive vapours (pyridine, deuterated acetonitrile, acetone, *etc.*) and non-reactive gases ($CO_2$ and CO) are also promising molecular probes because their size permits the access to the required pore size range and they only titrate the strong and moderate acid sites.[58] Infrared (IR) spectroscopy has often been applied to identify these acid sites by studying the interactions between the acid sites and the adsorbed probe molecules.[63]

**Pyridine.** The most widely used probe for this IR technique is pyridine, whose adsorption can be easily detected by IR spectroscopy. Pyridine adsorption onto the UMCs of MOFs will lead to the formation of extra peaks in the corresponding IR spectra. For example, Volkringer *et al.* introduced pyridine into MIL-100(Al) (MIL = Matérial Institut Lavoisierat) at 573 K to probe its Lewis acidity.[64] After applying vacuum at 373 K to remove physisorbed pyridine, the corresponding IR spectrum displayed three peaks at 1018, 1051, and 1074 $cm^{-1}$, which could be assigned to the $\nu_1$, $\nu_{12}$, and $\nu_{18a}$ modes of pyridine that had been coordinated to the $Al^{3+}$ UMCs, respectively (Fig. 9). The total amount of pyridine only coordinated to $Al^{3+}$ UMCs can be calculated using the molar absorption coefficients of the $\nu_{12}$ and $\nu_{18a}$ bands.

**Deuterated acetonitrile.** Acetonitrile, a small molecule with low basicity ($pK_b$ = 24), also shows great potential in

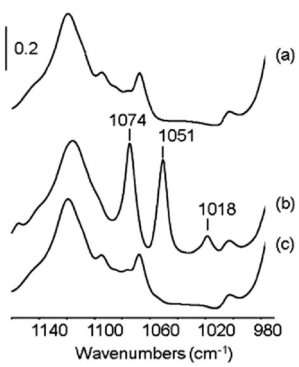


Fig. 9 Infrared spectra: (a) activated MIL-100(Al); (b) after pyridine adsorption (133 Pa at equilibrium pressure) at 373 K followed by evacuation at the same temperature; (c) recycled MIL-100(Al) by outgassing at 553 K.[64] Reprinted with permission from the American Chemical Society, copyright 2012.

determining the strong acid sites in solid materials.[65] It is better to use deuterated acetonitrile ($CD_3CN$) for this application, which gives a less complex IR spectrum because $\nu$(CN) vibration is not perturbed by Fermi resonance.[65] In one example, the $CD_3CN$ molecules adsorbed on MIL-100(Al) lead to two main $\nu$(CN) bands (Fig. 10), suggesting the presence of physisorbed [$\nu$(CN) = 2263 $cm^{-1}$] and coordinated [$\nu$(CN) = 2321 $cm^{-1}$] $CD_3CN$ species on $Al^{3+}$ UMC.[64,65] The band at 2114 $cm^{-1}$ was ascribed to the $\nu(CD_3)$ vibration of adsorbed $CD_3CN$. After evacuation, the intensity of the $\nu$(CN) band because of the physisorbed species strongly decreased (Fig. 10b), while the intensity of the band of acetonitrile that was coordinated onto the $Al^{3+}$ sites slightly decreased and shifted to 2326 $cm^{-1}$. Evacuation at higher temperatures (Fig. 10c–e) suggested a new weak $\nu$(CN) band at 2341 $cm^{-1}$ (shoulder), which was assigned to Al defects with stronger Lewis acidity. In the $\nu$(CH) range, the intensity of the framework band at 3058 $cm^{-1}$ strongly decreased in the presence of acetonitrile, while witnessing the growth of the band at 3078 $cm^{-1}$. The IR spectrum could return to its original shape after the complete removal of adsorbed acetonitrile.

**Acetone.** Similar to pyridine, acetone can be used as a probe molecule to weigh the acidity of the UMCs of MOFs as well. Hong *et al.* studied the interactions between acetone and $M_2$(dobpdc) (M = Mn, Co, Ni, Zn; dobpdc = 4,4′-dihydroxy-1,1′-biphenyl-3,3′-dicarboxylic acid) *via* IR spectroscopy.[66] The C═O stretching bands were observed at 1709.6, 1708.6, 1706.7, and 1709.1 $cm^{-1}$ for acetone molecules binding to Mn, Co, Ni, and Zn UMCs, respectively, while the band at 1715.0 $cm^{-1}$ was for free acetone (Fig. 11). Since coordination of acetone onto the UMCs will lead to an elongated C═O bond, the $\Delta\nu$(C═O) value can reflect the relative Lewis acidity of the UMCs in MOFs.[67] In the above case, the Lewis acidity increases from Mn to Ni UMCs and then decreases for the Zn UMC.

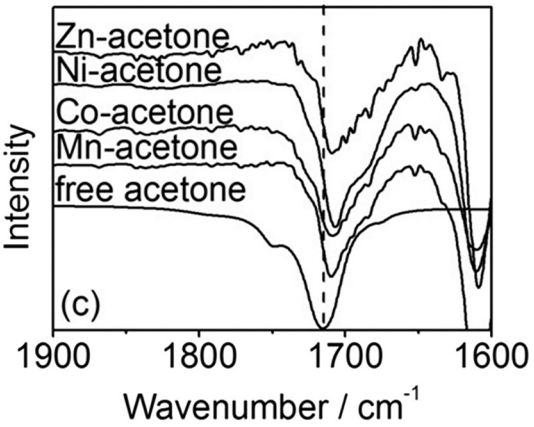


Fig. 11 *In situ* IR characterization of MOF–acetone interactions.[66] Reprinted with permission from Wiley-VCH, copyright 2016.

**Carbon monoxide (CO).** CO is a weak soft Lewis base with a small molecular size (3.69 Å) and can be used as an unreactive probe at low temperatures (77 K and 100 K).[63] Vimont *et al.* studied the interactions between CO and MIL-100(Al) with an increase in CO dose at 100 K.[64] The initial addition of CO (56 μmol $g^{-1}$) boosted the increase in the intensity of the $\nu$(CO) band at 2210 $cm^{-1}$ (Fig. 12). Further addition of CO did not increase its intensity but led to an additional band at 2195 $cm^{-1}$, whose intensity increased and wavenumber shifted to 2183 $cm^{-1}$ (parts b–d of Fig. 12). After saturation, a weak band at 2154 $cm^{-1}$ and two strong bands at 2138 and 2135 $cm^{-1}$ appeared because of physisorbed CO species. Regarding the hydroxyl vibrations, CO loading shifted the band at 3588 $cm^{-1}$ (weak) toward a lower wavenumber and gave rise to a broader band at 3510 $cm^{-1}$ (Fig. 12, inset). Similar to aluminium oxide, the weak $\nu$(CO) band at 2210 $cm^{-1}$ could be due to the crystal defects of strong Lewis acidity, while the main $\nu$(CO) band at 2195–2184 $cm^{-1}$ corresponded to the CO adsorption on a large amount

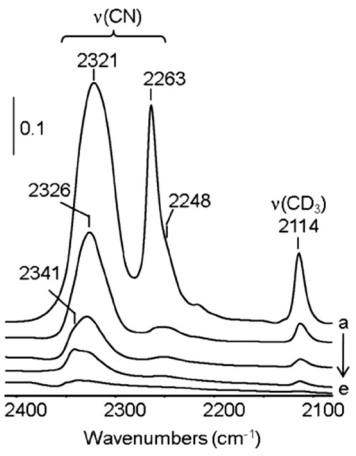


Fig. 10 Infrared spectra of activated MIL-100(Al): (a) after introduction of $CD_3CN$ into the cell (9330 Pa), followed by evacuation at (b) room temperature, (c) 323 K, (d) 373 K, and (e) 423 K.[64] Reprinted with permission from the American Chemical Society, copyright 2012.

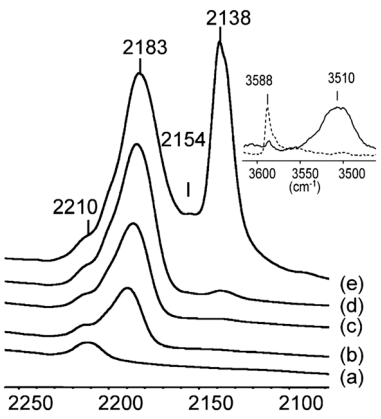


Fig. 12 IR spectra of MIL-100(Al) recorded at 100 K and outgassed at 373 K (a); after increasing the CO dose from 56 μmol $g^{-1}$ (b) to 900 μmol $g^{-1}$ (d); at an equilibrium pressure (1333 Pa) (e). Inset: spectrum of MIL-100(Al) activated at 573 K before (dotted line) and after (solid line) introducing an equilibrium pressure of CO at 100 K.[64] Reprinted with permission from the American Chemical Society, copyright 2012.

 

of $Al^{3+}$ UMCs resulting from the removal of water molecules.[68]

Besides qualitative evaluation of the strength of Lewis or Brønsted acidity, IR studies of CO adsorption can also be employed for quantitative analysis as long as the molar absorption coefficients are known for Lewis or Brønsted acid sites.[69] In these studies, CO needs to be doped by calibrated aliquots at 100 K in order to measure the $\nu$(CO) molar absorption coefficient by assuming that the CO will only adsorb on the surface at a low coverage under such conditions. In one study, the introduction of CO on the activated MIL-100(Al) provoked a linear increase in the intensity of the band at 2195–2184 $cm^{-1}$ (Fig. 13), corresponding to the CO coordinated to $Al^{3+}$ UMCs. Its molar absorption coefficient was calculated to be 2.0 μmol $g^{-1}$ cm based on the slope of the trend line and was irrelevant to the activation temperature. The value of the adsorption coefficient in the above study is similar to the reported value for $\nu$(CO) bands based on $Cr^{3+}$ UMCs in MIL-100(Cr).[69] Given the measured molar absorption coefficient, the number of corresponding $Al^{3+}$ UMCs can be probably determined for different activation temperatures. In the above example, the amount of CO molecules coordinated onto the UMCs reaches 2.2 mmol $g^{-1}$ for the sample activated at 623 K.

### 3.3 Isosteric heats of adsorption

Carbon dioxide ($CO_2$), because of its high polarizability ($29.11 \times 10^{25}$ $cm^3$) and quadrupole moment ($4.3 \times 10^{26}$ esu $cm^2$),[70] can also be used to qualitatively evaluate the Lewis acidity of MOFs.[71] In one study, the $CO_2$ uptakes of Mn, Co, Ni, and Zn based MOF-74 reached 43.5, 42.0, 60.18, and 31.4 $cm^3$ $g^{-1}$, respectively, under a partial pressure of 0.15 bar at 298 K (Fig. 14a).[66] Ni-MOF-74 exhibited the highest $CO_2$ uptake among the above series, indicating its highest Lewis acid strength. Besides, the heat of $CO_2$ adsorption can also be used to evaluate the Lewis acid strength.[31] For example, the zero-coverage $CO_2$ heats of adsorption were found to be 25.0, 33.9, 34.5, and 25.6 kJ $mol^{-1}$ for Mn, Co, Ni, and Zn MOF-74, respectively (Fig. 14b), confirming the strongest Lewis acid strength of Ni-MOF-74.

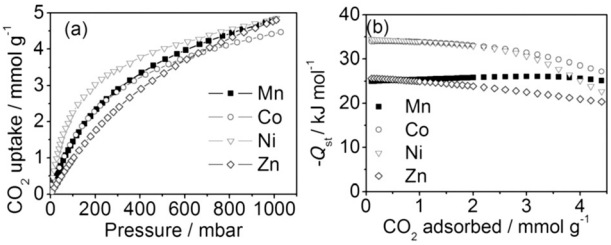


Fig. 14 (a) $CO_2$ isotherms of the MOF-74 series at 298 K. (b) Isosteric heats of $CO_2$ adsorption in the MOF-74 series.[66] Reprinted with permission from Wiley-VCH, copyright 2016.

Besides $CO_2$, other small molecules that can have Lewis acid–base interactions with MOFs can also be utilized to probe the Lewis acid strength. For example, Mukherjee and coworkers reported the π-complexation triggered Lewis acid–base interactions between benzene and MOF-74.[72] They performed the single component benzene and cyclohexane vapour sorption experiments at 298 K for the entire series of MOF-74. Mn and Ni based MOF-74 showed the highest benzene uptake capacity. However, the adsorption strength between these molecules and MOFs remains to be studied.

### 3.4 Density functional theory calculations

The strength of Lewis acid sites in MOFs can also be evaluated by density functional theory (DFT) calculations using basic molecules as the probe. For example, Liu *et al.* studied the interactions between CO and HKUST-1 using DFT calculations.[73] It was observed that CO could be adsorbed through either the C (Fig. 15a) or the O end (Fig. 15b), which however depends on the initial structural arrangement in the optimization process. The axis of the adsorbed CO molecule is parallel to the axis of Cu UMCs, with an adsorption energy of 6.63 or 3.14 kcal $mol^{-1}$ for adsorption through the C or O end, respectively. This result indicated that CO molecules tended to adsorb onto the Cu UMCs of HKUST-1 through Cu–C adsorption.[74] A further DFT study on the strength of Lewis sorption sites is suggested to optimize the geometry parameters, natural bond orbital (NBO) charge, vibrational frequency and adsorption energy of probe molecules.[73]

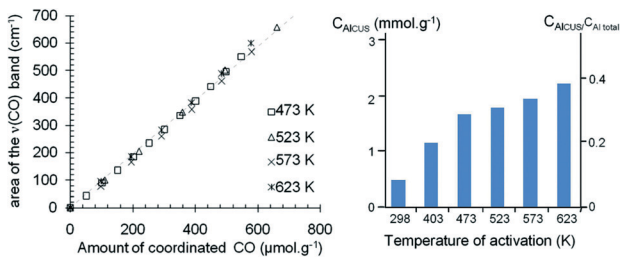


Fig. 13 Integrated area of $\nu$(CO) bands (2170–2220 $cm^{-1}$ range) *versus* the introduced CO concentration into the IR cell at 100 K (left) under different activation temperatures; concentration of $Al^{3+}$ UMCs *versus* activation temperature (right).[64] Reprinted with permission from the American Chemical Society, copyright 2012.

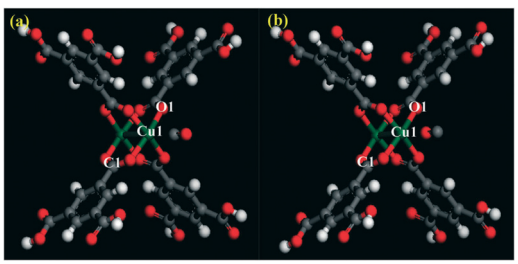


Fig. 15 The local structures of the CO molecule adsorbed on the Cu UMCs of HKUST-1: (a) C end adsorption; (b) O end adsorption[73] (Cu, green; O, red; C, gray; H, white). Reprinted with permission from the American Chemical Society, copyright 2010.

# 4. Typical catalytic applications

MOFs with UMCs can act as Lewis acid catalysts and have been attempted for various reactions (Table 1), such as addition, reduction, oxidation, cyclization, substitution, hydrogenation, host–guest interaction, *etc.*[75,76] In this section, we will highlight several typical reactions using MOFs as the catalysts.

## 4.1 Addition reaction

**Cyanosilylation.** Cyanosilylation is a common addition reaction, in which nitrile groups and silyl groups are added across double bonds or triple bonds catalysed by Lewis acids (Fig. 16).[77] The mechanism is as follows: (1) the oxygen of aldehydes coordinates onto the Lewis acid sites; (2) nitrile groups attack the carbonyl groups; (3) silyl groups isomerize to form cyanohydrin. For example, our group has previously reported the use of meso-HKUST-1 MOFs as Lewis acid catalysts for cyanosilylation reaction of benzaldehyde.[10] We found that the mesopores introduced within meso-HKUST-1 could facilitate the substrate transport and make it highly accessible to catalytically active Cu sites. Another interesting study was reported by Mo and co-workers.[78] They prepared a homochiral MOF based on an enantiopure 2,2′-dihydroxy-1,1′-biphenyl ligand. After exchanging the protons of the dihydroxyl group with $Li^+$, the resultant MOF demonstrated high efficiency and recyclability in catalysing asymmetric cyanation of aromatic aldehydes with >99% enantiomeric excess (ee).

**Prins reaction.** The Prins reaction is an electrophilic addition reaction of aldehydes to alkenes or ketones followed by capture of a nucleophile facilitated by Lewis acid catalysts (Fig. 17).[79] Opanasenko *et al.* carried out the Prins addition reaction of β-pinene and paraformaldehyde to produce nopol using aluminosilicate zeolites, titanosilicate zeolite MFI, and a series of MOFs as the catalysts.[80] They found that the activity of the investigated MOFs increased with an increase in the strength of Lewis acidity in the following increasing order: ZIF-8 < MIL-53(Al) < FeBTC < MIL-100(Cr) < MIL-100(Fe). Moreover, the presence of Brønsted acid sites within zeolites resulted in side products, which decreased the selectivity compared to the reactions catalysed by MOFs. In addition, when using MIL-100(Fe) as the catalyst, the nopol yield also increased with an increase in solvent polarity.

Table 1 Summary of MOFs for Lewis acid catalysis applications

| No. | Reaction type | Specific reaction |
|---|---|---|
| 1 | Addition | Cyanosilylation |
| | | Prins reaction |
| | | Strecker reaction |
| 2 | Redox | Photochemical $CO_2$ reduction |
| | | Electrochemical $CO_2$ reduction |
| | | Hydrocarbon oxidation |
| | | Water oxidation |
| 3 | Cyclization | $CO_2$ cyclization reaction |
| 4 | Substitution | Friedel–Crafts reaction |
| 5 | Hydrogenation | Hydrogenation of alkenes |
| | | Hydrogenation of $CO_2$ |
| 6 | Dehydration | Fructose, glucose |
| 7 | Isomerization | |
| 8 | Host–guest interaction | |

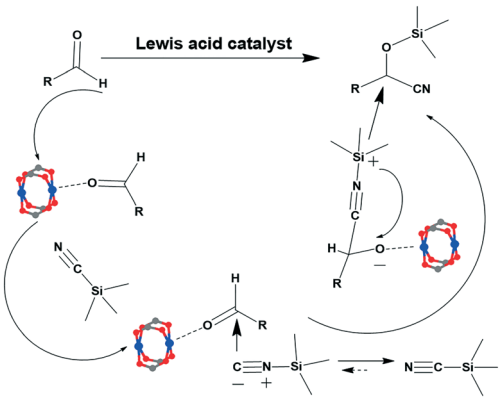


Fig. 16 Scheme of cyanosilylation catalysed by MOFs.

**Strecker reaction.** The Strecker reaction is very useful in the synthesis of amino acids and α-aminonitriles, where aldehydes or ketones are condensed with ammonium chloride or amines in the presence of cyanides to form α-aminonitriles, which can be subsequently hydrolyzed to produce amino acids (Fig. 18).[81] Monge *et al.* conducted several studies using MOFs as the catalysts for one-pot three-component Strecker reactions of aldehydes and ketones.[82,83] In one example, they reported a mesoporous In MOF (InPF-110) with a high density of active metal sites, affording excellent catalytic activity in the formation of substituted α-aminonitriles through the one-pot Strecker reaction of ketones at room temperature.[83] In addition, this MOF catalyst could be reused for up to 10 cycles without any observable loss of activity.

## 4.2 Redox reaction

**Photochemical $CO_2$ reduction.** The excessive $CO_2$ emission into the atmosphere has caused global climate deterioration and thus needs to be properly addressed by carbon capture and conversion.[84] Direct conversion of $CO_2$ into hydrocarbon

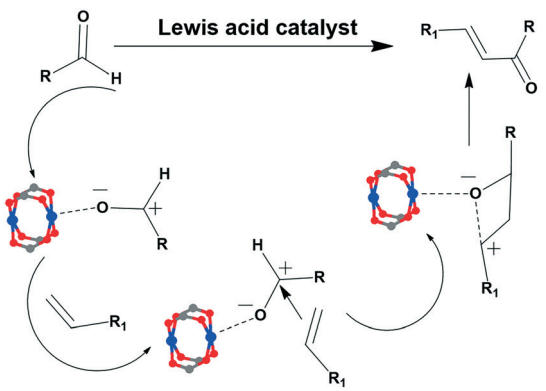


Fig. 17 Scheme of the Prins reaction catalysed by MOFs.

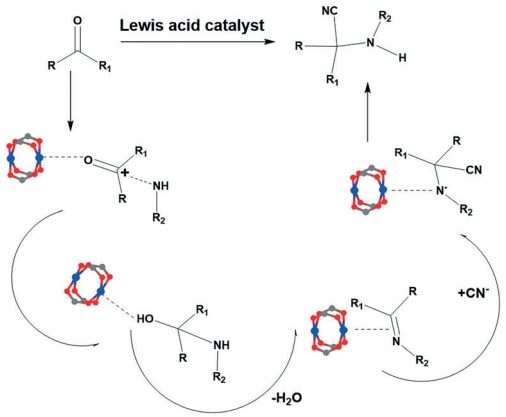


Fig. 18 Scheme of the Strecker reaction catalysed by MOFs.

fuels using sunlight is an exciting solution, which can reduce the $CO_2$ emission and produce renewable fuels simultaneously.[85] Conventional $TiO_2$-based photocatalysts have been widely investigated owing to their superior stability, availability, and low material cost.[86] However, their $CO_2$ photoreduction efficiency is far from satisfactory, mainly because of the low $CO_2$ adsorption capacity as well as their limited activity (only UV active) under the full solar spectrum.[87] Because of the presence of versatile metal clusters, which can serve as semiconductor quantum entities as well as Lewis sites for anchoring and activating $CO_2$ molecules,[87] MOFs have been studied for such conversions (Fig. 19). In order to reach good catalytic performance, MOFs should have excellent visible-light harvesting capability and favorable adsorption toward $CO_2$.[85]

Wang and co-workers demonstrated photocatalytic $CO_2$ reduction using UiO-67 doped with metal complexes (Ir, Re, and Ru) and obtained CO as the reduction product with a medium turnover number (TON, defined as the number of conversion of substrate molecules per catalytic active site) of 10.9 in 6 h and a low turnover frequency of $5.05 \times 10^{-5}$ $s^{-1}$ (TOF, defined as the number of conversion of substrate molecules per catalytic active site and per second).[88] In this system, the incorporation efficiency of metal sites is limited and

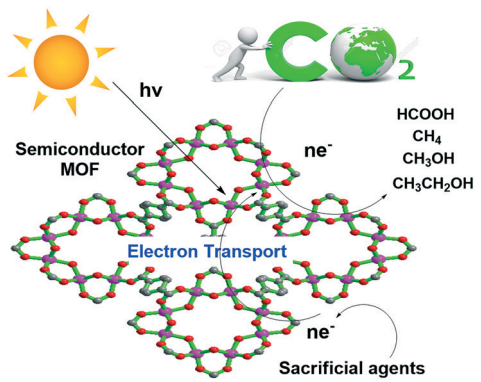


Fig. 19 Scheme of the photochemical $CO_2$ reduction catalysed by MOFs.

the recyclability of MOFs remains to be improved. Fu and co-workers synthesized MIL-125(Ti)-$NH_2$ and demonstrated its capability in the photocatalytic reduction of $CO_2$ to formic acid in acetonitrile under visible light irradiation with triethanolamine as the sacrificial agent.[89] Several MOFs and their composites are found to be photoactive, such as UiO-66(Zr)-$NH_2$,[90,91] NNU-28(Zr),[92] MOF-253(Ru),[93] PCN-222(Zr),[94] mixed metal based UiO-66(Zr/Ti)-$NH_2$,[95] UiO-66(Zr)-CrCAT and UiO-66(Zr)-GaCAT,[96] iron-based MILs,[97] Ru–polypyridine based MOF,[98] metal clusters incorporated UiO-67,[99–102] Co-ZIF-9,[103–105] UiO-66 loaded with carbon nitride nanosheets,[106] MIL-101(Fe)-derived iron nanoparticles,[107] *etc.* However, most of them can only reduce $CO_2$ to CO or formates. MOF/$TiO_2$ nanocomposites[108,109] and MOF-derived composites[110] have been found to be highly active for $CO_2$ reduction to methane in the presence of water. For example, Khaletskaya and co-workers pyrolyzed the composite containing gold nanoparticles (GNPs) and MIL-125(Ti)-$NH_2$ into gold/titania nanocomposites (GNP/$TiO_2$) for photocatalytic $CO_2$ reduction (Fig. 20).[110] With improved visible light absorption contributed by the gold surface plasmon, as well as increased electron storage capacities, the GNP-doped $TiO_2$ significantly increased the $CH_4$ yield, as compared to the $TiO_2$ references [P-25 and AUROlite (Au/$TiO_2$)].

**Electrochemical $CO_2$ reduction.** Electrochemical reduction of $CO_2$ in the presence of water into hydrocarbon compounds (methane, methanol) as fuels or chemical feedstocks is another attractive solution to mitigate the side effect of $CO_2$ emission.[111] Conventional electrocatalysts for $CO_2$ conversion have the limitations of large electrochemical overpotentials, poor long-term stability, and low faradaic efficiency (*i.e.* low product selectivity and yields, reduced $H_2$ productivity).[112] Small molecular porphyrin compounds chelated with transition metals are widely studied for electrochemical reduction of $CO_2$ due to their relatively high electronic conductivity, excellent catalytic efficiency, and easy availability.[112] In one recent example, depending on the pH values of electrolyte solutions (pH = 1, hydrogen evolution; pH = 3, water reduction), the underlying mechanism for electrochemical $CO_2$ reduction catalysed by a Co-containing porphyrin compound was generally divided into the following steps (Fig. 21):[113] (1) coordinated $CO_2$ on metal sites was reduced by electrons to form a Co complex, $CO_2 + e^- + M \rightarrow M\text{–}(CO_2)^-$; (2) the Co complex

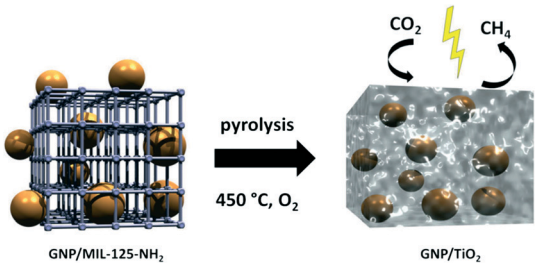


Fig. 20 Scheme for the preparation of gold/titania nanocomposites.[110] Reprinted with permission from the American Chemical Society, copyright 2015.

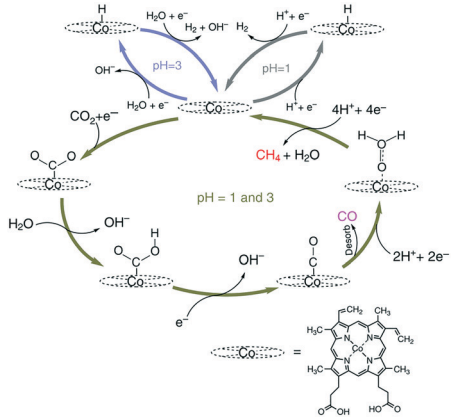


Fig. 21 Scheme of the electrochemical $CO_2$ reduction catalysed by cobalt porphyrin (Co-TCPP).[113] Reprinted with permission from Macmillan Publishers, 2015.

reacted with water to form a metal-bound carboxyhydroxyl intermediate, M–$(CO_2)^-$ + $H_2O$ → M–COOH + OH; (3) the carboxyhydroxyl intermediate was further reduced to generate CO, M–COOH + $e^-$ → M–CO + $OH^-$; (4) CO subsequently dissociated from the complex; (5) the CO was further reduced by two electrons into $CH_4$.

For MOFs to be used as good electrocatalysts, the electronic conductivity and activity of the immobilized transition metal sides (Fe, Co, Mn, *etc.*) are the key factors to be considered. Compared with homogeneous molecular porphyrin catalysts, embedding porphyrin moieties into porous materials such as MOFs has the potential advantages of fully exposed active sites. In order to enhance the electron transport, several studies have been conducted to deposit MOF thin films onto conductive substrates. For example, Hod and co-workers deposited an Fe-porphyrin based MOF thin film onto fluorine doped tin oxide (FTO) glass substrates and achieved an ~100% faradaic efficiency for $CO_2$ reduction into CO and $H_2$ mixtures.[114] Yaghi and co-workers used porphyrin-based framework materials for electrocatalytic $CO_2$ reduction to CO in water.[115,116]

Although porphyrin-based MOFs demonstrate a high catalytic efficiency toward CO or $CH_4$, to further reduce $CO_2$ into more rewarding high-energy-density alcohol fuels (methanol and ethanol) requires the use of other metal-based catalytic systems, such as Cu-MOFs,[117,118] Zn-MOFs,[119] *etc.* Among all the active metal sites, Cu is regarded as the most promising one for such conversion because it is capable of producing hydrocarbons with high reaction rates.[120] However, Cu catalysts usually generate a wide range of products with low selectivity.[121] One breakthrough example was made by Albo and co-workers,[117] who prepared stable metal–organic aerogels using Cu as the active site for electrocatalytic $CO_2$ reduction into alcohols (Fig. 22). The maximum production rates of $CH_3OH$ and $C_2H_5OH$ for HKUST-1 as the electrodes were 5.62 × $10^{-6}$ mol $m^{-2}$ $s^{-1}$ and 5.28 × $10^{-6}$ mol $m^{-2}$ $s^{-1}$, respectively. However, the maximum cumulative faradaic efficiency (FE) for $CO_2$ reduction is below 15% and the long-term stability of Cu-MOFs remains to be further studied.

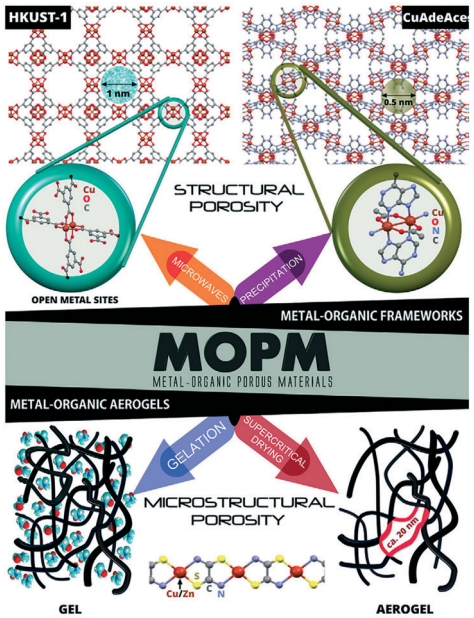


Fig. 22 Metal–organic aerogels containing Cu as the active sites for electrocatalytic $CO_2$ reduction into alcohols.[117] Reprinted with permission from Wiley-VCH, copyright 2016.

**Hydrocarbon oxidation.** The selective oxidation of carbon–hydrogen bonds is an important reaction to produce ketones and carboxylic acids.[122] Due to the availability of highly redox-active metal sites (*e.g.* iron, chromium), MOFs can be easily tailored for such reactions.[123] Dhakshinamoorthy *et al.* studied the oxidation reaction of aromatic carbons into ketones catalysed by MIL-100(Fe).[124] Another interesting example was demonstrated by Long and co-workers, who systematically studied the effects of the local hydrophobic environment on the product selectivity of cyclohexane oxidation catalysed by expanded analogues of Fe-MOF-74 with exposed $Fe^{2+}$ sites (Fig. 23).[125] They have demonstrated that a 3-fold enhancement of the alcohol-to-ketone product ratio and an order of magnitude increase in TON could be achieved by altering the pore size and installing nonpolar hydrophobic functional groups near the iron centers. Besides Fe-based MOFs, other metal (W, Ru) loaded Zr-based MOFs have also been used for hydrocarbon oxidation reactions.[126,127]

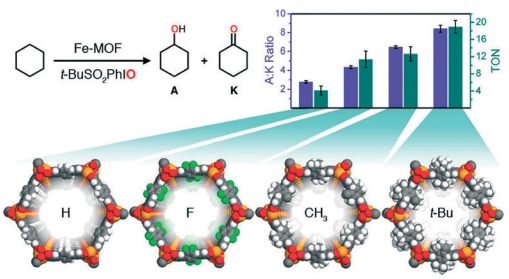


Fig. 23 Oxidation of cyclohexane to cyclohexanol and cyclohexanone catalysed by Fe-based MOFs.[125] Reprinted with permission from the American Chemical Society, copyright 2016.

 

**Water oxidation.** The solar-driven water splitting into hydrogen is a promising solution for the energy issue involved nowadays. The most challenging step for this process is water oxidation (aka oxygen evolution reaction, OER) because it requires a minimum potential of 1.23 V to oxidize $O^{2-}$ into $O_2$ ($2H_2O \rightarrow O_2 + 4H^+ + 4e^-$).[128] Currently, the OER driven by solar energy is largely limited by its sluggish kinetics and highly efficient OER catalysts are urgently needed. MOFs can act as potential candidates for such applications due to the presence of UMCs capable of lowering the energy barrier as well as tunable organic linkers to harvest sunlight and transfer electrons efficiently.[129] For example, Chi and co-workers investigated the feasibility of several Fe-based MOFs, MIL-53(Fe), MIL-88B(Fe), and MIL-101(Fe), for photocatalytic OER under visible light irradiation (Fig. 24).[130] Among these MOFs, MIL-101(Fe) exhibited superior OER activities over other Fe-based MOFs in basic solutions.

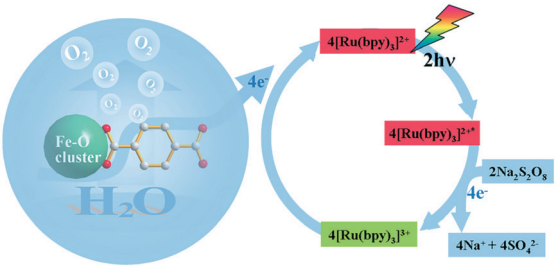


Fig. 24 Scheme of the photocatalytic water oxidation catalysed by Fe-based MOFs.[130] Reprinted with permission from Wiley-VCH, copyright 2016.

### 4.3 $CO_2$ cyclization reaction

Besides $CO_2$ reduction, using $CO_2$ as a feedstock for the synthesis of useful cyclic carbonates by the cyclization reactions between epoxides and $CO_2$ is another important solution to mitigate the effect of $CO_2$ emission.[131] Conventional approaches have the limitations of low catalyst stability and reactivity under high pressure and temperature conditions, air sensitivity, and use of co-solvents.[132] Salen[133] and porphyrin[134,135] based MOFs loaded with transition metals (Zn, Co, Ni) have been widely attempted for such conversion. The proposed mechanism for $CO_2$ cyclization into carbonates catalysed by Lewis acids is shown in Fig. 25:[136–138] (1) epoxides coordinate onto the Lewis acid sites; (2) the co-catalyst tetraalkylammonium bromide (TAAB) attacks the partially negative oxygen; (3) $CO_2$ inserts into the O–A bonds; (4) cyclization reactions; (5) cyclic carbonates detach. The first step for such conversion is the rate determining step for epoxide activation to form ammonia ions for subsequent insertion of $CO_2$, and catalysts with strong Lewis acidity are preferred.[138]

Cu,[139–141] Zn,[142] and Hf (ref. 143) based MOFs with strong Lewis acid sites have also been applied for such reactions. For example, Li and co-workers reported a Cu-based MOF with both exposed metal sites and nitrogen-rich triazole groups, showing high affinity toward $CO_2$ molecules and

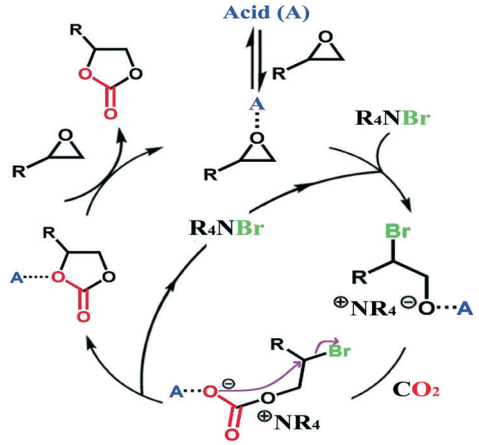


Fig. 25 Proposed mechanism for Lewis acid (A) catalysed cyclic carbonate synthesis from epoxides and $CO_2$ in the presence of a TAAB co-catalyst.[137] Reprinted with permission from Wiley-VCH, copyright 2016.

good catalytic performance for $CO_2$ cycloaddition at room temperature and 1 bar (Fig. 26).[144] In addition, they showed a size-dependent selectivity toward small epoxide substrates because of the pore confinement. Zhang and co-workers synthesized a highly robust sulfonate-based Cu-MOF, TMOF-1, which was stable over a wide pH range as well as boiling in aqueous solutions.[141] TMOF-1 exhibited a nearly quantitative yield in converting 2-methyloxirane to the corresponding cyclic carbonate, which was significantly higher than that of the benchmark Cu-MOF, HKUST-1.

### 4.4 Friedel–Crafts substitution reaction

There are mainly two types of Friedel–Crafts reactions: alkylation and acylation reactions, both of which proceed by electrophilic aromatic substitution in the presence of Lewis acid catalysts.[145,146] MOFs, such as Zn-MOF-5,[147] Cu-MOF-74,[148] Zr-MOF,[149] Fe-MOF,[150] *etc.*, have also been attempted for these reactions. Zhang and co-workers designed a stable Cu-MOF through a post-synthetic metal exchange reaction

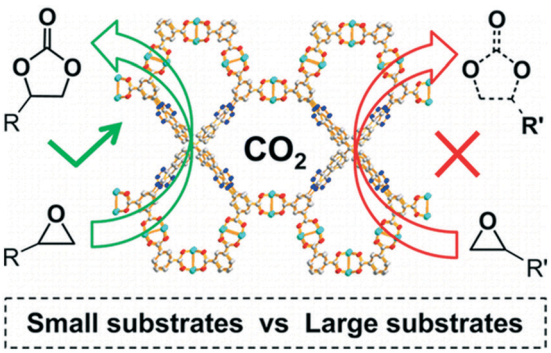


Fig. 26 Cu-MOF with UMCs and nitrogen-rich triazole groups for catalytic $CO_2$ cycloaddition.[144] Reprinted with permission from the American Chemical Society, copyright 2016.

from its Zn(II) analogue (Fig. 27).[151] The resultant Cu-MOF demonstrated superior catalytic efficiency for Friedel–Crafts reaction between indole and substituted b-nitrostyrenes over its Zn(II) analogue.

### 4.5 Hydrogenation reaction

**Hydrogenation of alkenes.** Hydrogenation is an important type of reaction to produce saturated hydrocarbons, aldehydes, and alcohols.[111] In this process, the unsaturated hydrocarbons have to be adsorbed onto the surface of metal catalysts, where Lewis acid sites help activate the alkenes and split hydrogen atoms.[152] One of the reported strategies to produce MOF catalysts for such a reaction is to embed and disperse metal nanoparticles (MNPs) into porous MOF supports, wherein the catalytic activity of MNPs can be largely increased by maximizing the exposed active sites within MOFs.[153] For example, Somorjai *et al.* reported a series of MOFs incorporating platinum metal nanocrystals, and their application in catalysing gas-phase hydrogenation of methylcyclopentane.[154,155] Jiang[156] and Lin[157] groups also reported the loading of metal particles or clusters into stable UiO-series MOFs for selective hydrogenation of alkenes.

**Hydrogenation of $CO_2$.** Besides the hydrogenation of unsaturated hydrocarbons, hydrogenative reduction of $CO_2$ is another promising solution for the pressing global environmental issues.[111] In the catalytic process, Lewis acid sites are believed to be capable of binding $CO_2$ and dissociating $H_2$.[158] Ye and co-workers conducted computational calculations of using pristine and modified UiO-66 for $CO_2$ hydrogenation into formates[159] and methanol.[160] Rungtaweevoranit and co-workers incorporated 18 nm Cu nanocrystals (NCs) into the single crystals of UiO-66 (Cu⊂UiO-66), which were capable of reducing $CO_2$ to methanol (Fig. 28).[161] $CO_2$ hydrogenation conducted at 175 °C and 10 bar ($CO_2:H_2 = 1:3$, molar ratio) revealed that only Cu⊂UiO-66, Cu on UiO-66, Cu on $ZrO_2$, and Cu/ZnO/$Al_2O_3$ could convert $CO_2$ to methanol, and Cu⊂UiO-66 had the highest TOF of $3.7 \times 10^{-3}$ $s^{-1}$. Neither Cu NCs on MIL-101 (Cr) nor Cu NCs⊂ZIF-8 showed catalytic activity, indicating that the catalysts only work being supported by $ZrO_2$ or ZnO. They demonstrated that the superior catalytic activity and selectivity of the Cu NC catalyst originated from strong interactions between Cu NCs and Zr secondary building units (SBUs) of MOFs, supported by X-ray photoelectron spectroscopy (XPS) results wherein the Zr 3d binding energy shifted toward the lower oxidation state in the presence of Cu NCs. This is the first finding that SBUs of MOFs can have a strong metal–support interaction as typically observed in bulk metal oxides, which offers a new insight to integrate metal nanoclusters into MOFs for highly efficient and selective $CO_2$ hydrogenation into fuels.

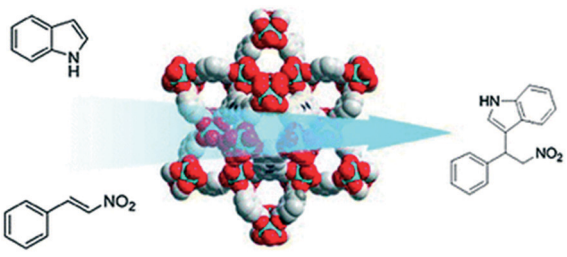


Fig. 27 Cu-MOF for Friedel–Crafts reaction.[145] Reprinted with permission from the Royal Society of Chemistry, copyright 2016.

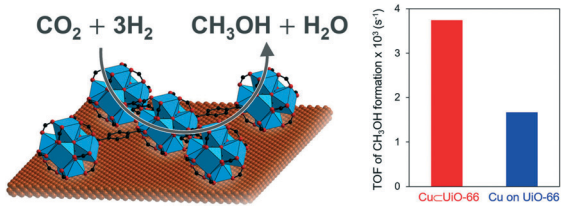


Fig. 28 Scheme for hydrogenative reduction of $CO_2$ to methanol using Cu nanocrystals into UiO-66 single crystals (Cu⊂UiO-66).[161] Reprinted with permission from the American Chemical Society, copyright 2016.

### 4.6 Dehydration reaction

Acid-promoted dehydration reactions of glucose and fructose from biomass are important processes in preparing platform chemicals such as 5-hydroxymethylfurfural (HMF) for further synthesis of other chemicals.[162] Unlike the dehydration of fructose that only requires Brønsted acid catalysts, the conversion of glucose is more challenging and requires a hybrid catalytic system including both Lewis and Brønsted acidity.[163,164] This reaction goes as follows: (1) glucose firstly isomerizes to fructose catalysed by Lewis acids; (2) fructose dehydrates to HMF catalysed by Brønsted acids (Fig. 29). Currently, the most efficient system for such conversion is $CrCl_2$-based Lewis acid catalysts in the presence of ionic liquids.[162] However, it suffers from moisture-related deactivation, high cost, and low recyclability.[163] Compared to other catalytic systems, MOFs are tunable in both the Lewis acid site and the Brønsted acid site.[20] So far, MOFs with a pure Lewis acid site are not found to be catalytically active for glucose

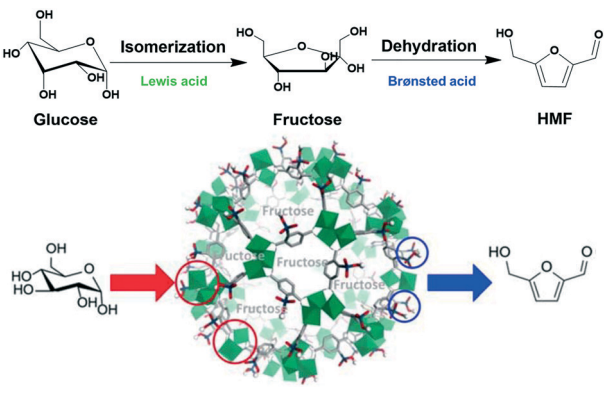


Fig. 29 Scheme for the Lewis acid–Brønsted acid bifunctional catalyst MIL-101(Cr)-$SO_3H$ for glucose conversion to HMF.[165] Reprinted with permission from John Wiley and Sons, copyright 2016.

 

dehydration. Su *et al.* reported a hybrid MOF, MIL-101(Cr)-$SO_3H$, containing both a strong Lewis acid site from $Cr^{3+}$ and a Brønsted acid site from $-SO_3H$ groups, for glucose conversion, resulting in a HMF yield of 44.9% and a selectivity of 45.8% (Fig. 29).[165] This work represents a sustainable and green process for bifunctional MOF-involved catalytic glucose conversion to platform chemicals.

### 4.7 Isomerization reaction

Isomerization is a catalytic process by which one molecule is transformed into another one having the same elemental composition but with different atomic arrangements.[166] When the isomerization occurs intramolecularly, it is also considered as a rearrangement reaction. MOFs with Lewis acidity can also be applied for such a reaction. For example, Dhakshinamoorthy and co-workers investigated a series of $Fe^{3+}$-containing MOFs, including the commercial Basolite F-300 and synthesized MIL-88B(Fe), MIL-88C(Fe), MIL-100(Fe), and MIL-127(Fe), as the catalysts for α-pinene oxide rearrangement into camphonelal and isopinocamphone in the absence of a solvent (Fig. 30).[167] About 10% conversion with 50% selectivity toward camphonelal and ~40% selectivity toward isopinocamphone was obtained for the best MOF catalyst, Basolite F-300, which had also shown catalytic activity toward the rearrangement of other epoxides (norbornene oxides).

### 4.8 Host–guest interaction

Lithium–sulfur (Li–S) batteries are one of the most promising energy storage systems due to its high specific capacity of 1675 mA h $g^{-1}$ and energy density of 2650 W h $kg^{-1}$ as well as low material cost.[168] Li–S batteries operate by electrochemical reduction of sulfur (during discharge) into lithium polysulfides with different chain lengths, which will finally form insoluble $Li_2S_2$ or $Li_2S$.[168] The major issue preventing them from practical applications is the "shuttle effect" due to dissolution of the discharge/charge intermediates (sulfur or polysulfides) in organic electrolytes, resulting in significant capacity loss of the sulfur cathodes and poor cycle life of the batteries.[168] One promising route to address these issues is to develop porous composite cathode materials capable of immobilizing polysulfides by encapsulating sulfur in porous carriers.[169] MOFs are therefore gaining escalating attention in Li–S batteries because of their highly porous nature and tunable internal surface functionality for anchoring these polysulfides and help in stabilizing the reactive discharge/charge intermediates (polysulfides) in organic electrolytes.[169]

For example, Zheng and co-workers demonstrated that a Ni-MOF was remarkably capable of immobilizing polysulfides within the cathode through Lewis acid–base interactions, where the retention of energy capacity reached 89% after 100 cycles at 0.1 C.[170] Based on the same interaction, Wang and co-workers developed a zirconium–metalloporphyrin framework, MOF-525(Cu), as a host for the inclusion of sulfur and polysulfides in Li–S batteries.[171] The S@MOF-525(Cu) cathode has demonstrated a reversible capacity of ~700 mA h $g^{-1}$ at 0.5 C even after 200 cycles. Bai and co-workers reported an HKUST-1–graphene oxide (GO) composite separator as an ionic sieve in Li–S batteries, which selectively sieved $Li^+$ ions and efficiently suppressed undesired polysulfide migration to the anode side (Fig. 31).[172] When a sulfur-containing mesoporous carbon material (~70 wt% sulfur) was used as the cathode composite, the Li–S battery with the MOF-GO separator exhibited a low capacity decay rate (0.019% per cycle over 1500 cycles), with almost no capacity loss after the initial 100 cycles.

## 5. Summary and outlook

In this Highlight, we have reviewed the common strategies toward the design and synthesis of MOFs with Lewis acidity. Compared to traditional acid catalysts, such as zeolites and homogeneous metal catalysts, the generation of Lewis acid sites in MOFs is more designable and versatile. However, the key to address the Achilles' heel of MOF-based catalysts, *i.e.* weak thermal and chemical stability, for industrial applications, remains to be further explored. Currently, modulator-based synthetic approaches have been proven to be useful in generating Lewis acid sites inside stable UiO-series and MIL-series MOFs. However, several key issues remain to be resolved, such as how to maintain the high stability of the parent MOF structures in the derived MOFs to meet the industrial requirements. Other approaches to prepare MOFs with Lewis acidity remain to be further developed, such as preparing multivariate (MTV)[173] MOFs with different metals, ligands, or hybridized structures.[174]

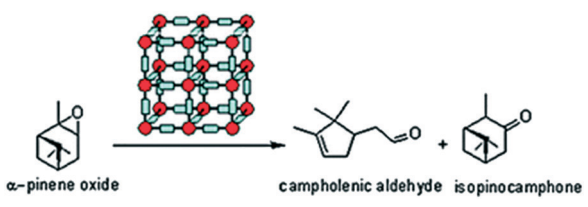


Fig. 30 Scheme for the isomerization (rearrangement) of α-pinene oxide into camphonelal and isopinocamphone using Fe-based MOFs.[167] Reprinted with permission from the Royal Society of Chemistry, copyright 2012.

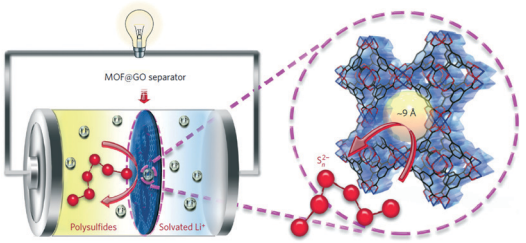


Fig. 31 Schematic illustration of the HKUST-1@GO separator used in Li–S batteries.[172] Reprinted with permission from Macmillan Publishers, copyright 2016.

The current characterization techniques for the detection and quantification of Lewis acid sites in MOFs are versatile but remain to be further improved. The $NH_3$-TPD technique has its limitation in quantifying the concentration of the Lewis acid site, while other techniques like IR studies and gas sorption studies cannot satisfy the needs to fundamentally understand the catalytic mechanism and quantify the active sites.[175] In the future, any improvement in the characterization techniques of Lewis acid sites is welcome and of particular interest in catalysis and analytic chemistry.

Currently, MOFs have been widely attempted for various reactions, such as addition, substitution, oxidation, and photo- or electrochemical reduction. The applications of MOFs in other catalytic reactions should be an indispensable aspect and highly beneficial to expand the scope of MOFs as catalytic materials.

## Acknowledgements

This work is supported by the National University of Singapore (CENGas R-261-508-001-646) and the Ministry of Education – Singapore (MOE AcRF Tier 2 R-279-000-429-112).

## References

1 A. Schoedel, M. Li, D. Li, M. O'Keeffe and O. M. Yaghi, *Chem. Rev.*, 2016, **116**, 12466–12535.
2 K. Sumida, D. L. Rogow, J. A. Mason, T. M. McDonald, E. D. Bloch, Z. R. Herm, T. H. Bae and J. R. Long, *Chem. Rev.*, 2012, **112**, 724–781.
3 B. Li, H.-M. Wen, W. Zhou and B. Chen, *J. Phys. Chem. Lett.*, 2014, **5**, 3468–3479.
4 C. Wang, X. Liu, N. Keser Demir, J. P. Chen and K. Li, *Chem. Soc. Rev.*, 2016, **45**, 5107–5134.
5 A. Dhakshinamoorthy, M. Alvaro and H. Garcia, *Chem. Commun.*, 2012, **48**, 11275–11288.
6 M. Fujita, Y. J. Kwon, S. Washizu and K. Ogura, *J. Am. Chem. Soc.*, 1994, **116**, 1151–1152.
7 K. Schlichte, T. Kratzke and S. Kaskel, *Microporous Mesoporous Mater.*, 2004, **73**, 81–88.
8 S. Horike, M. Dincă, K. Tamaki and J. R. Long, *J. Am. Chem. Soc.*, 2008, **130**, 5854–5855.
9 T. Ladrak, S. Smulders, O. Roubeau, S. J. Teat, P. Gamez and J. Reedijk, *Eur. J. Inorg. Chem.*, 2010, 3804–3812.
10 Z. Hu, Y. Peng, K. M. Tan and D. Zhao, *CrystEngComm*, 2015, **17**, 7124–7129.
11 L. H. Wee, C. Wiktor, S. Turner, W. Vanderlinden, N. Janssens, S. R. Bajpe, K. Houthoofd, G. Van Tendeloo, S. De Feyter, C. E. A. Kirschhock and J. A. Martens, *J. Am. Chem. Soc.*, 2012, **134**, 10911–10919.
12 Y. K. Hwang, D. Y. Hong, J. S. Chang, S. H. Jhung, Y. K. Seo, J. Kim, A. Vimont, M. Daturi, C. Serre and G. Ferey, *Angew. Chem., Int. Ed.*, 2008, **47**, 4144–4148.
13 M. Opanasenko, A. Dhakshinamoorthy, M. Shamzhy, P. Nachtigall, M. Horáček, H. Garcia and J. Čejka, *Catal. Sci. Technol.*, 2013, **3**, 500–507.
14 S. Marx, W. Kleist and A. Baiker, *J. Catal.*, 2011, **281**, 76–87.
15 V. Lykourinou, Y. Chen, X. S. Wang, L. Meng, T. Hoang, L. J. Ming, R. L. Musselman and S. Q. Ma, *J. Am. Chem. Soc.*, 2011, **133**, 10382–10385.
16 D. W. Feng, Z. Y. Gu, J. R. Li, H. L. Jiang, Z. W. Wei and H. C. Zhou, *Angew. Chem., Int. Ed.*, 2012, **51**, 10307–10310.
17 J. A. Johnson, J. Luo, X. Zhang, Y. S. Chen, M. D. Morton, E. Echeverria, F. E. Torres and J. Zhang, *ACS Catal.*, 2015, **5**, 5283–5291.
18 M. H. Beyzavi, R. C. Klet, S. Tussupbayev, J. Borycz, N. A. Vermeulen, C. J. Cramer, J. F. Stoddart, J. T. Hupp and O. K. Farha, *J. Am. Chem. Soc.*, 2014, **136**, 15861–15864.
19 J. C. Jiang, F. Gándara, Y. B. Zhang, K. Na, O. M. Yaghi and W. G. Klemperer, *J. Am. Chem. Soc.*, 2014, **136**, 12844–12847.
20 J. C. Jiang and O. M. Yaghi, *Chem. Rev.*, 2015, **115**, 6966–6997.
21 Z. Hu, Y. Peng, Y. Gao, Y. Qian, S. Ying, D. Yuan, S. Horike, N. Ogiwara, R. Babarao, Y. Wang, N. Yan and D. Zhao, *Chem. Mater.*, 2016, **28**, 2659–2667.
22 N. C. Burtch, H. Jasuja and K. S. Walton, *Chem. Rev.*, 2014, **114**, 10575–10612.
23 J. Canivet, A. Fateeva, Y. M. Guo, B. Coasne and D. Farrusseng, *Chem. Soc. Rev.*, 2014, **43**, 5594–5617.
24 Z. Wang, G. Chen and K. L. Ding, *Chem. Rev.*, 2009, **109**, 322–359.
25 J. Lee, O. K. Farha, J. Roberts, K. A. Scheidt, S. T. Nguyen and J. T. Hupp, *Chem. Soc. Rev.*, 2009, **38**, 1450–1459.
26 A. Corma, H. Garcia and F. X. L. Xamena, *Chem. Rev.*, 2010, **110**, 4606–4655.
27 Y. Liu, W. M. Xuan and Y. Cui, *Adv. Mater.*, 2010, **22**, 4112–4135.
28 W. Xuan, C. Zhu, Y. Liu and Y. Cui, *Chem. Soc. Rev.*, 2012, **41**, 1677–1695.
29 J. D. Evans, C. J. Sumby and C. J. Doonan, *Chem. Soc. Rev.*, 2014, **43**, 5933–5951.
30 J. Canivet, M. Vandichel and D. Farrusseng, *Dalton Trans.*, 2016, **45**, 4090–4099.
31 J. L. C. Rowsell and O. M. Yaghi, *J. Am. Chem. Soc.*, 2006, **128**, 1304–1315.
32 H. X. Deng, S. Grunder, K. E. Cordova, C. Valente, H. Furukawa, M. Hmadeh, F. Gándara, A. C. Whalley, Z. Liu, S. Asahina, H. Kazumori, M. O'Keeffe, O. Terasaki, J. F. Stoddart and O. M. Yaghi, *Science*, 2012, **336**, 1018–1023.
33 P. D. C. Dietzel, V. Besikiotis and R. Blom, *J. Mater. Chem.*, 2009, **19**, 7362–7370.
34 Z. Hu, S. Faucher, Y. Zhuo, Y. Sun, S. Wang and D. Zhao, *Chem. – Eur. J.*, 2015, **21**, 17246–17255.
35 J. Liu, L. Chen, H. Cui, J. Zhang, L. Zhang and C.-Y. Su, *Chem. Soc. Rev.*, 2014, **43**, 6011–6061.
36 Y. Sun, L. Sun, D. Feng and H.-C. Zhou, *Angew. Chem., Int. Ed.*, 2016, **55**, 6471–6475.
37 W. Liang, C. J. Coghlan, F. Ragon, M. Rubio-Martinez, D. M. D'Alessandro and R. Babarao, *Dalton Trans.*, 2016, **45**, 4496–4500.

 

38 H. Wu, Y. S. Chua, V. Krungleviciute, M. Tyagi, P. Chen, T. Yildirim and W. Zhou, *J. Am. Chem. Soc.*, 2013, **135**, 10525–10532.
39 P. Ghosh, Y. J. Colon and R. Q. Snurr, *Chem. Commun.*, 2014, **50**, 11329–11331.
40 G. C. Shearer, S. Chavan, J. Ethiraj, J. G. Vitillo, S. Svelle, U. Olsbye, C. Lamberti, S. Bordiga and K. P. Lillerud, *Chem. Mater.*, 2014, **26**, 4068–4071.
41 C. A. Trickett, K. J. Gagnon, S. Lee, F. Gándara, H.-B. Bürgi and O. M. Yaghi, *Angew. Chem., Int. Ed.*, 2015, **54**, 11162–11167.
42 M. J. Cliffe, W. Wan, X. Zou, P. A. Chater, A. K. Kleppe, M. G. Tucker, H. Wilhelm, N. P. Funnell, F.-X. Coudert and A. L. Goodwin, *Nat. Commun.*, 2014, **5**, 4176.
43 Z. Hu, A. Nalaparaju, Y. Peng, J. Jiang and D. Zhao, *Inorg. Chem.*, 2016, **55**, 1134–1141.
44 Z. Hu, Y. Peng, Z. Kang, Y. Qian and D. Zhao, *Inorg. Chem.*, 2015, **54**, 4862–4868.
45 Z. Hu and D. Zhao, *Dalton Trans.*, 2015, **44**, 19018–19040.
46 J. M. Taylor, T. Komatsu, S. Dekura, K. Otsubo, M. Takata and H. Kitagawa, *J. Am. Chem. Soc.*, 2015, **137**, 11498–11506.
47 C. K. Brozek and M. Dinca, *Chem. Soc. Rev.*, 2014, **43**, 5456–5467.
48 C. K. Brozek and M. Dincă, *J. Am. Chem. Soc.*, 2013, **135**, 12886–12891.
49 C. H. Lau, R. Babarao and M. R. Hill, *Chem. Commun.*, 2013, **49**, 3634–3636.
50 H. Fei and S. M. Cohen, *J. Am. Chem. Soc.*, 2015, **137**, 2191–2194.
51 S. Pullen, H. Fei, A. Orthaber, S. M. Cohen and S. Ott, *J. Am. Chem. Soc.*, 2013, **135**, 16997–17003.
52 H. Fei, J. Shin, Y. S. Meng, M. Adelhardt, J. Sutter, K. Meyer and S. M. Cohen, *J. Am. Chem. Soc.*, 2014, **136**, 4965–4973.
53 G. Barin, V. Krungleviciute, O. Gutov, J. T. Hupp, T. Yildirim and O. K. Farha, *Inorg. Chem.*, 2014, **53**, 6914–6919.
54 Y. Liu, J.-R. Li, W. M. Verdegaal, T.-F. Liu and H.-C. Zhou, *Chem. – Eur. J.*, 2013, **19**, 5637–5643.
55 S. Shimomura, S. Horike, R. Matsuda and S. Kitagawa, *J. Am. Chem. Soc.*, 2007, **129**, 10990–10991.
56 B. Joarder, S. Mukherjee, A. K. Chaudhari, A. V. Desai, B. Manna and S. K. Ghosh, *Chem. – Eur. J.*, 2014, **20**, 15303–15308.
57 B. Manna, S. Mukherjee, A. V. Desai, S. Sharma, R. Krishna and S. K. Ghosh, *Chem. Commun.*, 2015, **51**, 15386–15389.
58 P. J. Barrie, *Phys. Chem. Chem. Phys.*, 2008, **10**, 1688–1696.
59 M. J. Sandoval and A. T. Bell, *J. Catal.*, 1993, **144**, 227–237.
60 H. Jiang, Q. Wang, H. Wang, Y. Chen and M. Zhang, *ACS Appl. Mater. Interfaces*, 2016, **8**, 26817–26826.
61 C. Chen, L.-X. Cai, B. Tan, Y.-J. Zhang, X.-D. Yang and J. Zhang, *Chem. Commun.*, 2015, **51**, 8189–8192.
62 M. Niwa and N. Katada, *Catal. Surv. Asia*, 1997, **1**, 215–226.
63 J. Jiang and O. M. Yaghi, *Chem. Rev.*, 2015, **115**, 6966–6997.
64 C. Volkringer, H. Leclerc, J.-C. Lavalley, T. Loiseau, G. Férey, M. Daturi and A. Vimont, *J. Phys. Chem. C*, 2012, **116**, 5710–5719.
65 A. Vimont, J. C. Lavalley, A. Sahibed-Dine, C. Otero Areán, M. Rodríguez Delgado and M. Daturi, *J. Phys. Chem. B*, 2005, **109**, 9656–9664.
66 G. Y. Yoo, W. R. Lee, H. Jo, J. Park, J. H. Song, K. S. Lim, D. Moon, H. Jung, J. Lim, S. S. Han, Y. Jung and C. S. Hong, *Chem. – Eur. J.*, 2016, **22**, 7444–7451.
67 M. Higuchi, K. Nakamura, S. Horike, Y. Hijikata, N. Yanai, T. Fukushima, J. Kim, K. Kato, M. Takata, D. Watanabe, S. Oshima and S. Kitagawa, *Angew. Chem., Int. Ed.*, 2012, **51**, 8369–8372.
68 C. Morterra and G. Magnacca, *Catal. Today*, 1996, **27**, 497–532.
69 A. Vimont, H. Leclerc, F. Maugé, M. Daturi, J.-C. Lavalley, S. Surblé, C. Serre and G. Férey, *J. Phys. Chem. C*, 2007, **111**, 383–388.
70 Z. Hu, K. Zhang, M. Zhang, Z. Guo, J. Jiang and D. Zhao, *ChemSusChem*, 2014, **7**, 2791–2795.
71 W. G. Lu, W. M. Verdegaal, J. M. Yu, P. B. Balbuena, H. K. Jeong and H. C. Zhou, *Energy Environ. Sci.*, 2013, **6**, 3559–3564.
72 S. Mukherjee, B. Manna, A. V. Desai, Y. Yin, R. Krishna, R. Babarao and S. K. Ghosh, *Chem. Commun.*, 2016, **52**, 8215–8218.
73 D. Liu and C. Zhong, *J. Phys. Chem. Lett.*, 2010, **1**, 97–101.
74 L. Benco, T. Bucko, J. Hafner and H. Toulhoat, *J. Phys. Chem. B*, 2004, **108**, 13656–13666.
75 A. Dhakshinamoorthy and H. Garcia, *ChemSusChem*, 2014, **7**, 2392–2410.
76 T. Bligaard, R. M. Bullock, C. T. Campbell, J. G. Chen, B. C. Gates, R. J. Gorte, C. W. Jones, W. D. Jones, J. R. Kitchin and S. L. Scott, *ACS Catal.*, 2016, **6**, 2590–2602.
77 Z. Zhang, J. Chen, Z. Bao, G. Chang, H. Xing and Q. Ren, *RSC Adv.*, 2015, **5**, 79355–79360.
78 K. Mo, Y. Yang and Y. Cui, *J. Am. Chem. Soc.*, 2014, **136**, 1746–1749.
79 L. J. Dolby, *J. Org. Chem.*, 1962, **27**, 2971–2975.
80 M. Opanasenko, A. Dhakshinamoorthy, Y. K. Hwang, J.-S. Chang, H. Garcia and J. Čejka, *ChemSusChem*, 2013, **6**, 865–871.
81 Y. Liu, K. Mo and Y. Cui, *Inorg. Chem.*, 2013, **52**, 10286–10291.
82 L. M. Aguirre-Díaz, F. Gándara, M. Iglesias, N. Snejko, E. Gutiérrez-Puebla and M. Á. Monge, *J. Am. Chem. Soc.*, 2015, **137**, 6132–6135.
83 D. Reinares-Fisac, L. M. Aguirre-Díaz, M. Iglesias, N. Snejko, E. Gutiérrez-Puebla, M. Á. Monge and F. Gándara, *J. Am. Chem. Soc.*, 2016, **138**, 9089–9092.
84 US Department of Energy, 2016.
85 S. C. Roy, O. K. Varghese, M. Paulose and C. A. Grimes, *ACS Nano*, 2010, **4**, 1259–1278.
86 M. Dan-Hardi, C. Serre, T. Frot, L. Rozes, G. Maurin, C. Sanchez and G. Ferey, *J. Am. Chem. Soc.*, 2009, **131**, 10857–10859.
87 O. K. Varghese, M. Paulose, T. J. LaTempa and C. A. Grimes, *Nano Lett.*, 2009, **9**, 731–737.

88 C. Wang, Z. Xie, K. E. deKrafft and W. Lin, *J. Am. Chem. Soc.*, 2011, **133**, 13445–13454.
89 Y. Fu, D. Sun, Y. Chen, R. Huang, Z. Ding, X. Fu and Z. Li, *Angew. Chem., Int. Ed.*, 2012, **51**, 3364–3367.
90 C. Gomes Silva, I. Luz, F. X. Llabrés i Xamena, A. Corma and H. García, *Chem. – Eur. J.*, 2010, **16**, 11133–11138.
91 D. Sun, Y. Fu, W. Liu, L. Ye, D. Wang, L. Yang, X. Fu and Z. Li, *Chem. – Eur. J.*, 2013, **19**, 14279–14285.
92 D. Chen, H. Xing, C. Wang and Z. Su, *J. Mater. Chem. A*, 2016, **4**, 2657–2662.
93 D. Sun, Y. Gao, J. Fu, X. Zeng, Z. Chen and Z. Li, *Chem. Commun.*, 2015, **51**, 2645–2648.
94 H.-Q. Xu, J. Hu, D. Wang, Z. Li, Q. Zhang, Y. Luo, S.-H. Yu and H.-L. Jiang, *J. Am. Chem. Soc.*, 2015, **137**, 13440–13443.
95 Y. Lee, S. Kim, J. K. Kang and S. M. Cohen, *Chem. Commun.*, 2015, **51**, 5735–5738.
96 Y. Lee, S. Kim, H. Fei, J. K. Kang and S. M. Cohen, *Chem. Commun.*, 2015, **51**, 16549–16552.
97 D. Wang, R. Huang, W. Liu, D. Sun and Z. Li, *ACS Catal.*, 2014, **4**, 4254–4260.
98 S. Zhang, L. Li, S. Zhao, Z. Sun and J. Luo, *Inorg. Chem.*, 2015, **54**, 8375–8379.
99 H. Fei, M. D. Sampson, Y. Lee, C. P. Kubiak and S. M. Cohen, *Inorg. Chem.*, 2015, **54**, 6821–6828.
100 M. B. Chambers, X. Wang, N. Elgrishi, C. H. Hendon, A. Walsh, J. Bonnefoy, J. Canivet, E. A. Quadrelli, D. Farrusseng, C. Mellot-Draznieks and M. Fontecave, *ChemSusChem*, 2015, **8**, 603–608.
101 T. Kajiwara, M. Fujii, M. Tsujimoto, K. Kobayashi, M. Higuchi, K. Tanaka and S. Kitagawa, *Angew. Chem., Int. Ed.*, 2016, **55**, 2697–2700.
102 K. Choi, D. Kim, B. Rungtaweevoranit, C. A. Trickett, J. T. D. Barmanbek, P. Yang and O. M. Yaghi, *J. Am. Chem. Soc.*, 2017, **139**, 356–362.
103 S. Wang, W. Yao, J. Lin, Z. Ding and X. Wang, *Angew. Chem., Int. Ed.*, 2014, **53**, 1034–1038.
104 S. Wang, J. Lin and X. Wang, *Phys. Chem. Chem. Phys.*, 2014, **16**, 14656–14660.
105 S. Wang and X. Wang, *Appl. Catal., B*, 2015, **162**, 494–500.
106 L. Shi, T. Wang, H. Zhang, K. Chang and J. Ye, *Adv. Funct. Mater.*, 2015, **25**, 5360–5367.
107 H. Zhang, T. Wang, J. Wang, H. Liu, T. D. Dao, M. Li, G. Liu, X. Meng, K. Chang, L. Shi, T. Nagao and J. Ye, *Adv. Mater.*, 2016, **28**, 3703–3710.
108 M. Wang, D. Wang and Z. Li, *Appl. Catal., B*, 2016, **183**, 47–52.
109 R. Li, J. Hu, M. Deng, H. Wang, X. Wang, Y. Hu, H.-L. Jiang, J. Jiang, Q. Zhang, Y. Xie and Y. Xiong, *Adv. Mater.*, 2014, **26**, 4783–4788.
110 K. Khaletskaya, A. Pougin, R. Medishetty, C. Rösler, C. Wiktor, J. Strunk and R. A. Fischer, *Chem. Mater.*, 2015, **27**, 7248–7257.
111 A. M. Appel, J. E. Bercaw, A. B. Bocarsly, H. Dobbek, D. L. DuBois, M. Dupuis, J. G. Ferry, E. Fujita, R. Hille, P. J. A. Kenis, C. A. Kerfeld, R. H. Morris, C. H. F. Peden, A. R. Portis, S. W. Ragsdale, T. B. Rauchfuss, J. N. H. Reek, L. C. Seefeldt, R. K. Thauer and G. L. Waldrop, *Chem. Rev.*, 2013, **113**, 6621–6658.
112 C. Costentin, S. Drouet, M. Robert and J.-M. Savéant, *Science*, 2012, **338**, 90–94.
113 J. Shen, R. Kortlever, R. Kas, Y. Y. Birdja, O. Diaz-Morales, Y. Kwon, I. Ledezma-Yanez, K. J. P. Schouten, G. Mul and M. T. M. Koper, *Nat. Commun.*, 2015, **6**, 8177.
114 I. Hod, M. D. Sampson, P. Deria, C. P. Kubiak, O. K. Farha and J. T. Hupp, *ACS Catal.*, 2015, **5**, 6302–6309.
115 S. Lin, C. S. Diercks, Y.-B. Zhang, N. Kornienko, E. M. Nichols, Y. Zhao, A. R. Paris, D. Kim, P. Yang, O. M. Yaghi and C. J. Chang, *Science*, 2015, **349**, 1208–1213.
116 N. Kornienko, Y. Zhao, C. S. Kley, C. Zhu, D. Kim, S. Lin, C. J. Chang, O. M. Yaghi and P. Yang, *J. Am. Chem. Soc.*, 2015, **137**, 14129–14135.
117 J. Albo, D. Vallejo, G. Beobide, O. Castillo, P. Castaño and A. Irabien, *ChemSusChem*, 2016, DOI: 10.1002/cssc.201600693.
118 R. Senthil Kumar, S. Senthil Kumar and M. Anbu Kulandainathan, *Electrochem. Commun.*, 2012, **25**, 70–73.
119 X. Kang, Q. Zhu, X. Sun, J. Hu, J. Zhang, Z. Liu and B. Han, *Chem. Sci.*, 2016, **7**, 266–273.
120 J. Qiao, Y. Liu, F. Hong and J. Zhang, *Chem. Soc. Rev.*, 2014, **43**, 631–675.
121 K. P. Kuhl, E. R. Cave, D. N. Abram and T. F. Jaramillo, *Energy Environ. Sci.*, 2012, **5**, 7050–7059.
122 H. Liu, Y. Li, H. Jiang, C. Vargas and R. Luque, *Chem. Commun.*, 2012, **48**, 8431–8433.
123 D. J. Xiao, E. D. Bloch, J. A. Mason, W. L. Queen, M. R. Hudson, N. Planas, J. Borycz, A. L. Dzubak, P. Verma, K. Lee, F. Bonino, V. Crocellà, J. Yano, S. Bordiga, D. G. Truhlar, L. Gagliardi, C. M. Brown and J. R. Long, *Nat. Chem.*, 2014, **6**, 590–595.
124 A. Dhakshinamoorthy, M. Alvaro, P. Horcajada, E. Gibson, M. Vishnuvarthan, A. Vimont, J.-M. Grenèche, C. Serre, M. Daturi and H. Garcia, *ACS Catal.*, 2012, **2**, 2060–2065.
125 D. J. Xiao, J. Oktawiec, P. J. Milner and J. R. Long, *J. Am. Chem. Soc.*, 2016, **138**, 14371–14379.
126 X.-L. Yang, L.-M. Qiao and W.-L. Dai, *Microporous Mesoporous Mater.*, 2015, **211**, 73–81.
127 X. Yu and S. M. Cohen, *Chem. Commun.*, 2015, **51**, 9880–9883.
128 J. D. Blakemore, R. H. Crabtree and G. W. Brudvig, *Chem. Rev.*, 2015, **115**, 12974–13005.
129 K. G. M. Laurier, F. Vermoortele, R. Ameloot, D. E. De Vos, J. Hofkens and M. B. J. Roeffaers, *J. Am. Chem. Soc.*, 2013, **135**, 14488–14491.
130 L. Chi, Q. Xu, X. Liang, J. Wang and X. Su, *Small*, 2016, **12**, 1351–1358.
131 A. Decortes, A. M. Castilla and A. W. Kleij, *Angew. Chem., Int. Ed.*, 2010, **49**, 9822–9837.
132 Y. Xie, T.-T. Wang, X.-H. Liu, K. Zou and W.-Q. Deng, *Nat. Commun.*, 2013, **4**, 1960.
133 Y. Ren, X. Cheng, S. Yang, C. Qi, H. Jiang and Q. Mao, *Dalton Trans.*, 2013, **42**, 9930–9937.

 

134 W. Jiang, J. Yang, Y.-Y. Liu, S.-Y. Song and J.-F. Ma, *Chem. – Eur. J.*, 2016, **22**, 16991–16997.
135 D. Feng, W.-C. Chung, Z. Wei, Z.-Y. Gu, H.-L. Jiang, Y.-P. Chen, D. J. Darensbourg and H.-C. Zhou, *J. Am. Chem. Soc.*, 2013, **135**, 17105–17110.
136 F. Castro-Gómez, G. Salassa, A. W. Kleij and C. Bo, *Chem. – Eur. J.*, 2013, **19**, 6289–6298.
137 H. He, J. A. Perman, G. Zhu and S. Ma, *Small*, 2016, **12**, 6309–6324.
138 M. H. Beyzavi, C. J. Stephenson, Y. Liu, O. Karagiaridi, J. T. Hupp and O. K. Farha, *Front. Energy Res.*, 2015, **2**, 63.
139 V. Guillerm, J. WeselińskiŁukasz, Y. Belmabkhout, A. J. Cairns, V. D'Elia, Ł. Wojtas, K. Adil and M. Eddaoudi, *Nat. Chem.*, 2014, **6**, 673–680.
140 W.-Y. Gao, Y. Chen, Y. Niu, K. Williams, L. Cash, P. J. Perez, L. Wojtas, J. Cai, Y.-S. Chen and S. Ma, *Angew. Chem., Int. Ed.*, 2014, **53**, 2615–2619.
141 G. Zhang, G. Wei, Z. Liu, S. R. J. Oliver and H. Fei, *Chem. Mater.*, 2016, **28**, 6276–6281.
142 R. Zou, P.-Z. Li, Y.-F. Zeng, J. Liu, R. Zhao, H. Duan, Z. Luo, J.-G. Wang, R. Zou and Y. Zhao, *Small*, 2016, **12**, 2334–2343.
143 M. H. Beyzavi, R. C. Klet, S. Tussupbayev, J. Borycz, N. A. Vermeulen, C. J. Cramer, J. F. Stoddart, J. T. Hupp and O. K. Farha, *J. Am. Chem. Soc.*, 2014, **136**, 15861–15864.
144 P.-Z. Li, X.-J. Wang, J. Liu, J. S. Lim, R. Zou and Y. Zhao, *J. Am. Chem. Soc.*, 2016, **138**, 2142–2145.
145 J. K. Groves, *Chem. Soc. Rev.*, 1972, **1**, 73–97.
146 J. V. Alegre-Requena, E. Marques-Lopez, R. P. Herrera and D. D. Diaz, *CrystEngComm*, 2016, **18**, 3985–3995.
147 N. T. S. Phan, K. K. A. Le and T. D. Phan, *Appl. Catal., A*, 2010, **382**, 246–253.
148 G. Calleja, R. Sanz, G. Orcajo, D. Briones, P. Leo and F. Martínez, *Catal. Today*, 2014, **227**, 130–137.
149 T. L. H. Doan, T. Q. Dao, H. N. Tran, P. H. Tran and T. N. Le, *Dalton Trans.*, 2016, **45**, 7875–7880.
150 M. V. Shamzhy, M. V. Opanasenko, H. Garcia and J. Čejka, *Microporous Mesoporous Mater.*, 2015, **202**, 297–302.
151 X. Zhang, Z. Zhang, J. Boissonnault and S. M. Cohen, *Chem. Commun.*, 2016, **52**, 8585–8588.
152 G. C. Bond and P. B. Wells, in *Adv. Catal.*, Academic Press, 1965, vol. 15, pp. 91–226.
153 R. J. White, R. Luque, V. L. Budarin, J. H. Clark and D. J. Macquarrie, *Chem. Soc. Rev.*, 2009, **38**, 481–494.
154 K. Na, K. M. Choi, O. M. Yaghi and G. A. Somorjai, *Nano Lett.*, 2014, **14**, 5979–5983.
155 K. M. Choi, K. Na, G. A. Somorjai and O. M. Yaghi, *J. Am. Chem. Soc.*, 2015, **137**, 7810–7816.
156 G. Huang, Q. Yang, Q. Xu, S.-H. Yu and H.-L. Jiang, *Angew. Chem., Int. Ed.*, 2016, **55**, 7379–7383.
157 K. Manna, T. Zhang, M. Carboni, C. W. Abney and W. Lin, *J. Am. Chem. Soc.*, 2014, **136**, 13182–13185.
158 D. W. Stephan and G. Erker, *Angew. Chem., Int. Ed.*, 2010, **49**, 46–76.
159 J. Ye and J. K. Johnson, *ACS Catal.*, 2015, **5**, 2921–2928.
160 J. Ye and J. K. Johnson, *Catal. Sci. Technol.*, 2016, **6**, 8392–8405.
161 B. Rungtaweevoranit, J. Baek, J. R. Araujo, B. S. Archanjo, K. M. Choi, O. M. Yaghi and G. A. Somorjai, *Nano Lett.*, 2016, **16**, 7645–7649.
162 M. E. Zakrzewska, E. Bogel-Łukasik and R. Bogel-Łukasik, *Chem. Rev.*, 2011, **111**, 397–417.
163 Y. J. Pagán-Torres, T. Wang, J. M. R. Gallo, B. H. Shanks and J. A. Dumesic, *ACS Catal.*, 2012, **2**, 930–934.
164 M. Moreno-Recio, J. Santamaría-González and P. Maireles-Torres, *Chem. Eng. J.*, 2016, **303**, 22–30.
165 Y. Su, G. Chang, Z. Zhang, H. Xing, B. Su, Q. Yang, Q. Ren, Y. Yang and Z. Bao, *AIChE J.*, 2016, **62**, 4403–4417.
166 J. D. Roberts and M. C. Caserio, *Basic Principles of Organic Chemistry*, 2nd edn, W. A. Benjamin, Inc., 1977.
167 A. Dhakshinamoorthy, M. Alvaro, H. Chevreau, P. Horcajada, T. Devic, C. Serre and H. Garcia, *Catal. Sci. Technol.*, 2012, **2**, 324–330.
168 P. G. Bruce, S. A. Freunberger, L. J. Hardwick and J.-M. Tarascon, *Nat. Mater.*, 2012, **11**, 19–29.
169 Z. W. Seh, J. H. Yu, W. Li, P.-C. Hsu, H. Wang, Y. Sun, H. Yao, Q. Zhang and Y. Cui, *Nat. Commun.*, 2014, **5**, 5017.
170 J. Zheng, J. Tian, D. Wu, M. Gu, W. Xu, C. Wang, F. Gao, M. H. Engelhard, J.-G. Zhang, J. Liu and J. Xiao, *Nano Lett.*, 2014, **14**, 2345–2352.
171 Z. Wang, B. Wang, Y. Yang, Y. Cui, Z. Wang, B. Chen and G. Qian, *ACS Appl. Mater. Interfaces*, 2015, **7**, 20999–21004.
172 S. Bai, X. Liu, K. Zhu, S. Wu and H. Zhou, *Nat. Energy*, 2016, **1**, 16094.
173 H. Deng, C. J. Doonan, H. Furukawa, R. B. Ferreira, J. Towne, C. B. Knobler, B. Wang and O. M. Yaghi, *Science*, 2010, **327**, 846–850.
174 K. A. McDonald, J. I. Feldblyum, K. Koh, A. G. Wong-Foy and A. J. Matzger, *Chem. Commun.*, 2015, **51**, 11994–11996.
175 H. Nguyen, V. Nikolakis and D. G. Vlachos, *ACS Catal.*, 2016, **6**, 1497–1504.